



HAL
open science

Crystallization by selective evaporation using membrane pervaporation: Application to l-glutamic acid to control polymorphism

Maya Khellaf, Xiaoqian Huang, Jean-Pierre Valour, Denis Mangin, Catherine Charcosset, Elodie Chabanon

► To cite this version:

Maya Khellaf, Xiaoqian Huang, Jean-Pierre Valour, Denis Mangin, Catherine Charcosset, et al.. Crystallization by selective evaporation using membrane pervaporation: Application to l-glutamic acid to control polymorphism. *Journal of Membrane Science*, 2023, 668, pp.121256. 10.1016/j.memsci.2022.121256 . hal-04049057

HAL Id: hal-04049057

<https://hal.science/hal-04049057v1>

Submitted on 17 Oct 2024

HAL is a multi-disciplinary open access archive for the deposit and dissemination of scientific research documents, whether they are published or not. The documents may come from teaching and research institutions in France or abroad, or from public or private research centers.

L'archive ouverte pluridisciplinaire **HAL**, est destinée au dépôt et à la diffusion de documents scientifiques de niveau recherche, publiés ou non, émanant des établissements d'enseignement et de recherche français ou étrangers, des laboratoires publics ou privés.

1
2 Crystallization by selective evaporation
3 using membrane pervaporation:
4 Application to L-glutamic acid to control
5 polymorphism

6
7 **Maya KHELLAF, Xiaoqian HUANG, Jean-Pierre VALOUR, Denis MANGIN, Catherine**
8 **CHARCOSSET, Elodie CHABANON***

9
10
11 Univ Lyon, Université Claude Bernard Lyon 1, CNRS, LAGEPP UMR 5007, 43
12 boulevard du 11 Novembre 1918, F-69100, VILLEURBANNE, France

13
14
15 *Article submitted to the*
16 *Journal of Membrane Science – August 2022*

17
18
19
20 *: Corresponding author

21 ☎: +33 4 72 43 18 52

22 Email: elodie.chabanon@univ-lyon1.fr

23 **ABSTRACT**

24 Crystallization is an important unit operation in process industries, driven by supersaturation, i.e. the
25 solute concentration difference between solution and equilibrium. Hence, to finely control the product
26 qualities, controlling mass and/or heat transfer is crucial. Membrane pervaporation, based on a
27 selective evaporation technique, appears as a process able to limit phase transition and control
28 polymorphism. In this work, a semi-continuous system is developed for the crystallization of L-glutamic
29 acid, which has two polymorphic forms. Hydrophilic HybSi[®] membranes are chosen. The influence of
30 different operating parameters on process performance in terms of solvent separation, solute
31 crystallization and control of polymorphism is investigated. Results validate the proof of concept and
32 highlight the preferential crystallization of a polymorphic form over the other. Hence, the α -form is
33 usually favoured except when the β -form is seeded, or at high temperature. Temperature appears as
34 the parameter influencing mostly the membrane selectivity and the polymorph generated. However,
35 concentration polarization and fouling, due to the deposit of L-glutamic acid crystals on the membrane
36 surface, are reported and decrease the process performance. Both phenomena are caused by a high
37 local supersaturation close to the membrane surface in addition to a local cooling due to the water
38 evaporation during pervaporation.

39 **KEYWORDS**

40 Pervaporation, membrane crystallization process, HybSi[®] membrane, polymorphism control, L-
41 glutamic acid

42 **1. INTRODUCTION**

43 Crystallization is one of the most important unit operations used to produce, purify or separate solid
44 products. The pharmaceutical industry is a major area of application for crystallization as about 90%
45 of pharmaceuticals contain active ingredients in the crystalline form [1,2]. The ordered structure of
46 crystals facilitates the rejection of impurities, making purification steps energy-efficient and cost-
47 effective. However, the compounds to be crystallized may adopt a different structural conformation
48 of the crystal lattice while being molecularly identical. This phenomenon is known as polymorphism.
49 Two polymorphic forms have different physical, mechanical and thermal properties (melting point,
50 density, compressibility, shape, solubility, dissolution rate, friability, purity...). These differences can
51 have a significant influence on the stability and bioavailability of the active ingredient, but also the
52 processing capability of the product in downstream processes (filtration, drying and processing). Due
53 to the therapeutic objectives of the manufactured products, the control of the crystallization process
54 is crucial in the pharmaceutical industry as a separation process of intermediates and as a final step in
55 the production of active ingredients. Batch crystallization in stirred reactors is the oldest approach and
56 remains the predominant method today [3]. Despite its robustness, it has some limitations such as
57 heterogeneities at the micro-mixing scale affecting the repeatability of the production, the
58 homogeneity of the final product from batch to batch and even the polymorphic phase crystallized [4].
59 For this purpose, membrane processes have been recently proposed as an alternative to improve
60 crystallization performance. They are often studied as tools for intensifying conventional processes
61 because they offer a good selectivity, large surface area per unit of volume, and the ability to control
62 contact and/or mixing between two phases [5]. Applied to crystallization, membrane processes would
63 allow the control of nucleation and growth kinetics, fast crystallization rates, good control of
64 supersaturation levels and polymorphism [6,7]. According to several pioneering studies, membrane
65 processes appear to be a tool to achieve these goals [8–10]. Di Profio et al. were among the first to

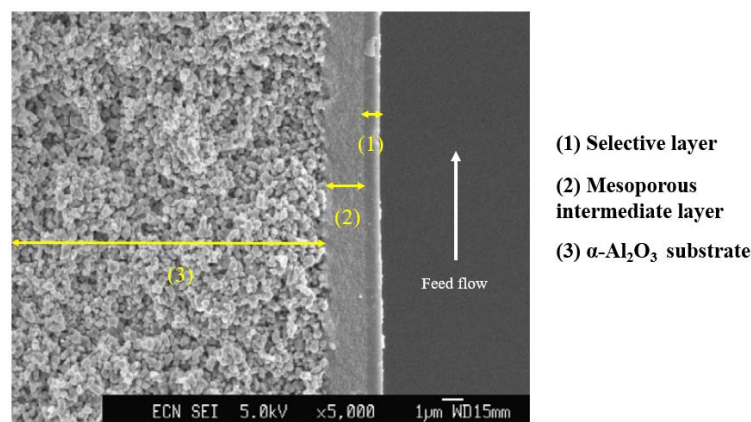
66 publish studies on the crystallization of active ingredients by membrane processes. In particular, they
67 studied the case of polymorphic forms of glycine [11,12], paracetamol [8,11,13] and carbamazepine
68 [13,14] by developing membrane crystallizers where the porous membrane matrix acts as a selective
69 barrier for solvent evaporation, modulating the final degree and rate of supersaturation generation.
70 Among the membrane processes of growing interest, pervaporation is chosen in this study as an
71 innovative process for crystallization. Pervaporation is generally used for separating a liquid mixture
72 by selective transfer through a dense membrane, where the constituents permeate and undergo a
73 change of state by vaporizing [15]. In the pharmaceutical field, it is mainly used for effluent
74 dehydration, solvent recovery and water removal during reactions [16–20]. As far as crystallization is
75 concerned, this technique remains relatively unexplored, despite the industrial potential of an
76 intensified process. Indeed, crystallization using membrane pervaporation would allow a better
77 control of the mass transfer, through the selective evaporation of the solvent thus providing the
78 supersaturation necessary to drive crystallization [7]. Several studies are being conducted to develop
79 new membrane materials applicable to pervaporation for the improvement of separation properties
80 of organic or hydro-organic mixtures [21,22]. However, only a few studies have reported the use of
81 pervaporation for the crystallization of organic compounds. The first mentioning the combination of
82 these two processes dates back more than a century ago when Kober reported the pervaporation
83 phenomenon through a dense membrane and introduced the percrystallization process [23]. It was
84 only years later that Bøddeker et al. [24] studied the sorption and pervaporation of vanillin from
85 aqueous solution. In another study by Zhang et al. and later by Li et al. [25,26], high-purity phenol
86 crystals (99.8%) were recovered from a dilute aqueous solution. These authors developed a two-stage
87 condenser system to collect the permeate containing phenol crystals using PEBAX membranes [25].
88 More recently, Zeng et al. [27] developed a two-step operation where pervaporation for water removal
89 is first conducted using NaA zeolite membrane, followed by a cooling crystallization and filtration to
90 collect sodium pyruvate and ethanol. However, performance limitations related to the use of
91 membrane technologies for crystallization have been reported in the literature. One of the major
92 obstacles is the problem of membrane fouling. This results in a decrease of membrane permeability
93 due to the deposition of suspended or dissolved components on the membrane surface [28]. Several
94 studies in the literature reported the influence of operating parameters on fouling. Indeed, Kieffer et
95 al. have shown that, for their experimental conditions, an increase in the inner diameter of the hollow
96 fibers was sufficient to reduce fouling, but no long-term experiments have been conducted [29]. Much
97 research has been carried out on membrane pre-treatment to limit fouling, based on the assumption
98 that wetting the membrane surface would avoid fouling effects [28,30–33]. Other researches have
99 been carried out on the use of cleaning solutions or additives to overcome fouling [34–37], but by
100 these means, it is more difficult to maintain the initial performance of the process and it may also
101 require the use of aggressive chemicals. Another phenomenon can lead to a significant decrease in
102 transmembrane flux : concentration polarization [38–40]. It corresponds to the formation of a
103 boundary layer of polar molecules on the membrane surface. The impact of concentration polarization
104 is specific to each separation process. The main factor influencing this phenomenon is the
105 hydrodynamics of the process. Indeed, increasing the flow velocity or using turbulence promoters
106 upstream of the membrane are technical means to decrease the thickness of the boundary layer.
107 This work aims to determine the operating parameters of the pervaporation process controlling the
108 final properties of the product to be crystallized (crystal size and polymorphic form) and to identify the
109 limiting parameters of the process. To achieve the objectives of this study, a semi-continuous
110 experimental setup has been developed. L-glutamic acid is chosen as a model compound as it

111 crystallizes under two well-known monotropic polymorphs: the stable β -polymorph (needle-like
112 shape) and the metastable α -polymorph (prismatic shape). The experimental results of this study have
113 highlighted the possibility of controlling the polymorphic form but also the limiting points of the
114 process operation.

115 2. MATERIALS & METHODS

116 2.1. Membranes and module

117 Organic/inorganic hybrid membranes HybSi[®] are used in this work. The HybSi[®] membrane is a hybrid
118 ceramic membrane [41–43] with a so-called "sandwich-like" structure (cf. Figure 1): i.e. a ceramic-
119 based substrate successively covered by an amorphous silica layer and a thin selective layer of HybSi[®]
120 in which silane precursors, such as BTESE (bis(triethoxysilyl)ethane) or BTESM
121 (bis(triethoxysilyl)methane) are incorporated [41,44].



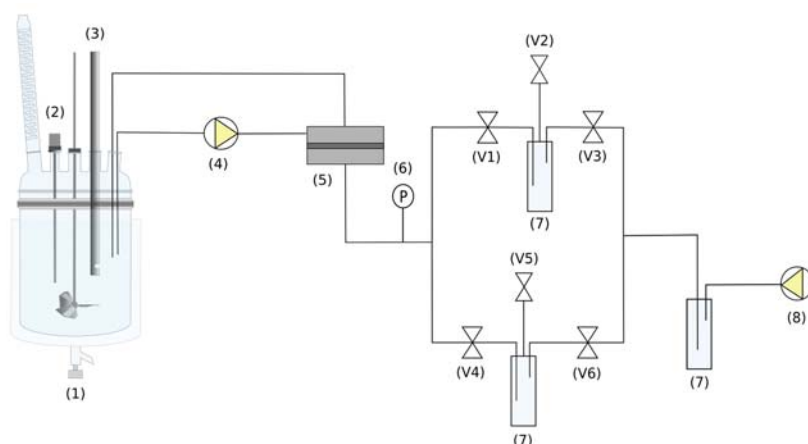
122

123 **Figure 1.** Cross-sectional SEM picture of HybSi[®] membrane [43]

124 For the following experiments, three tubular HybSi[®] membranes, purchased from Orelis Environment
125 (Alsys Group, France), are used. The membranes are from the same production batch and correspond
126 to the standard J05-A-X range with BTESM precursor. They are referred to M1, M2 and M3. The
127 membranes are monotubular with an internal diameter of 6mm, an external diameter of 10mm, a
128 length of 25cm and an effective area of 47cm².

129 2.2. Experimental setup

130 The experimental setup developed is shown in Figure 2.



131

132

Figure 2. Experimental setup for the crystallization pervaporation unit.

133 (1) Double jacketed 1L reactor; (2) Temperature probe; (3) EZ video probe; (4) Peristaltic pump; (5)
 134 Membrane module; (6) Pressure gauge; (7) Vacuum traps immersed in liquid nitrogen; (8) Vacuum
 135 pump; (V1-6) 2-way valves.

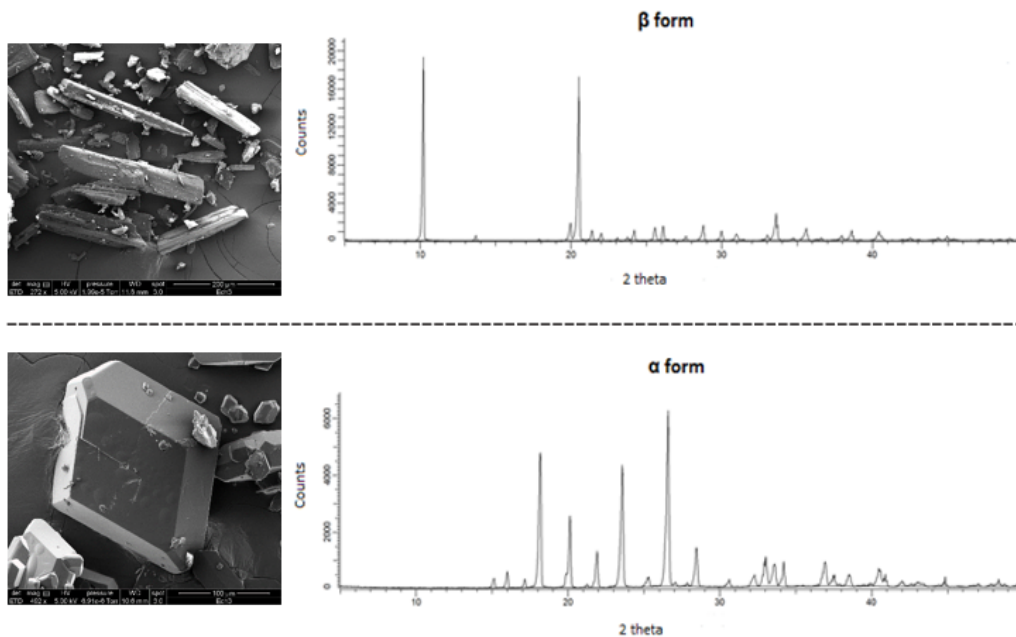
136 The feed mixture is put in a 1L double-jacketed reactor. The reactor temperature is controlled by a
 137 thermostatic bath (Ministat 230 Pilot One, Huber, Germany) equipped with a Pt100 temperature
 138 sensor. A 3-blade mixel TT[®] stainless steel propeller with a fixed speed of 400rpm provides stirring.
 139 The feed solution flows through a 10mm internal diameter polyvinyl chloride (PVC) tubing using a
 140 peristaltic pump (603S, Watson Marlow, UK) to the membrane module. The feed solution, at
 141 atmospheric pressure, flows on the lumen side of the tubular membrane. The retentate, i.e. the
 142 supersaturated solution after the selective evaporation of water, is reintroduced into the reactor. The
 143 permeate side is under vacuum allowing the selective transfer of water under vapour from the feed
 144 solution. The vacuum pressure, between 3 and 8mbar, is regulated by a PID controller and a Pirani
 145 capacitive gauge (0-100mbar, CMR362, Pfeiffer Vacuum, Germany) connected to a control unit (RVC
 146 300, Pfeiffer Vacuum, Germany). The vacuum pump is a vane pump (Adixen Pascal 2005SD, Pfeiffer
 147 Vacuum, Germany) with a nominal flow rate of 5.4m³/h and a total pressure limit closed (open) air
 148 ballast of 2.10⁻³mbar (10⁻²mbar). The permeate is then condensed in vacuum traps, immersed in liquid
 149 nitrogen, and regularly recovered during the experiment.

150 Hence, two vacuum traps are placed in parallel and operated alternately. A set of valves is used to
 151 switch between the two traps (cf. Figure 2). Finally, a safety trap, connected in series and operating
 152 continuously, is installed to protect the vacuum pump and to recover and quantify the permeate that
 153 is not condensed in the first trap.

154 2.3. Chemical products

155 For all experiments, the following products are used:

- 156 • Ultrapure water (Millipore Synergy[®] purification system, resistivity = 1.2mΩ.cm);
- 157 • Anhydrous absolute ethanol (Carlo Erba Reagent S.A.S, chemical purity ≥ 99.9%);
- 158 • β-polymorph of L-glu corresponding to the commercial product (Sigma Aldrich Co. Ltd, purity ≥
 159 99.5%);
- 160 • α-metastable form obtained according to the protocol previously described [45].



161

162 **Figure 3.** SEM micrographs and XRD patterns of the stable β -form and the metastable α -form of L-
 163 glutamic acid

164 Figure 3 presents the SEM micrographs and XRD patterns of both polymorphs. It is worth noting that,
 165 as expected, the α -form is prismatic while the β -form is needle-like. The XRD patterns show the
 166 presence of only one polymorph in each case with characteristic peaks at 10.2° 2 theta for the β -form
 167 and at 18.1° 2 theta for the α -form.

168 **2.4. Operating conditions and protocol**

169 A 1L of water/ethanol solution previously prepared by weighing (PM6000, Mettler Toledo, Germany)
 170 is introduced into the reactor. Three initial ethanol mass fractions ($w_{\text{EtOH,ini}}$) are investigated: 0.122,
 171 0.252 and 0.344. A precise amount of commercial L-glu is weighted and added to the solution. The
 172 amount of L-glu is calculated from the solubility data determined in a previous study [45], for an initial
 173 supersaturation fixed at 1.4 (cf. Table 1).

174 **Table 1.** Mass of L-glutamic acid added to the reactor according to the temperature and the
 175 composition

$w_{\text{EtOH,ini}}$ (-)	at 25°C		at 40°C	
	Solubility (g/kg of solution)	Mass added to the reactor (g)	Solubility (g/kg of solution)	Mass added to the reactor (g)
0.122	4.989	6.818	8.451	11.600
0.252	2.815	3.707	5.408	7.148
0.344	1.920	2.469	3.794	4.892

176 First, L-glu crystals are dissolved at a temperature of 20°C above the working temperature for about
 177 1h. The video probe immersed in the reactor monitors the dissolution of the crystals. The solution is
 178 then cooled to the working temperature. At the same time, the peristaltic pump is switched on at a
 179 fixed flow rate ($Q_v = 135\text{L/h}$, i.e. $Re > 7000$) to wet the membrane at the desired temperature for at
 180 least 45min before starting pervaporation. This is the time required to reach equilibrium between the
 181 membrane and the feed solution [46]. When the reactor temperature is stable, two samples of the

182 solution are taken, one is analysed using NMR to determine the initial ethanol mass fraction, and the
183 other is introduced into an oven at 85°C for 24h to determine the initial L-glu concentration of the
184 solution.

185 Then, the vacuum pump is switched on when the above conditions are set. Valves V1 and V3 are
186 opened and the experiment begins. Valves V2, V4, V5 and V6 remain closed (cf. Figure 2). Trap changes
187 are made every hour. The frequency of trap changes is optimised to avoid the risk of clogging.

188 Vacuum pressure and temperature are monitored every minute for the first 5min and then every
189 15min. At each trap change, a sample of the retentate is taken and analysed. The recovered trap is
190 warmed to room temperature to recover the frozen permeate. Once in a liquid state, the trap is
191 returned to atmospheric pressure through the V2 valve before being removed from the setup. The
192 permeate is then introduced into a glass vial and hermetically sealed. Vials are weighed before and
193 after on an analytical balance ($\pm 0.001\text{g}$, PM200, Mettler Toledo, Germany).

194 About 2mL of retentate is taken every 2h for analysis. A video is recorded before each trap change to
195 follow the appearance and growth of crystals in the reactor.

196 The experiments are carried out for 8h in order to follow the evolution and growth of the crystal and
197 any phase transitions.

198 At the end of the experiment, the L-glu suspension is removed. A heated ultrapure water solution is
199 added to the reactor and flows through the system. The membrane, the reactor and all the system
200 including the peristaltic pump and the tubes are cleaned with the heated water to dissolve and remove
201 L-glu residues. Lastly, the membrane, the reactor and all the system are washed with clean water
202 several times and dried at ambient temperature. To check the membrane regeneration, pervaporation
203 is carried out with a water/ethanol solution.

204 Several parameters are measured during the experiments. The total flux of permeate is determined
205 according to:

$$206 \quad J_{\text{tot}} = \frac{m_p}{S t} \quad \text{Eq.1}$$

207 Where J_{tot} is the total flux of permeate ($\text{kg}/(\text{m}^2 \cdot \text{h})$), m_p is the mass of permeate recovered in the trap
208 (g) for a period of time t (h) and S is the effective membrane area (m^2).

209 The permeate samples are then analysed by NMR to determine the mass fraction of ethanol and the
210 partial fluxes from the following equation:

$$211 \quad J_i = J_{\text{tot}} \cdot w_i^p \quad \text{Eq.2}$$

212 With J_i the partial flux of compound i (water or ethanol) ($\text{kg}/(\text{m}^2 \cdot \text{h})$) and w_i^p the mass fraction of
213 compound i (water or ethanol) in the permeate (-).

214 The separation factor, which quantitatively describes the quality of the separation, is defined by:

$$215 \quad \beta_{\text{water}/\text{EtOH}} = \frac{w_{\text{water}}^p / w_{\text{EtOH}}^p}{w_{\text{water}}^f / w_{\text{EtOH}}^f} \quad \text{Eq.3}$$

216 Where w_{water}^p and w_{EtOH}^p are the mass fractions respectively of water and ethanol in the permeate (-)
217) and w_{water}^f and w_{EtOH}^f in the feed solution (-).

218 The supersaturation factor, which describes the deviation of the L-glu concentration, noted C (in g.L⁻¹),
219 from its solubility, noted C* (in g.L⁻¹) is estimated by:

$$220 \quad \beta = \frac{C}{C^*} \quad \text{Eq.4}$$

221 **2.5. Characterization methods**

222 **2.5.1. In situ observation with the EZ video probe**

223 A video probe (EZProbe® 12005) is immersed in the stirred suspension and allows real-time
224 monitoring: before the experiment, to check the complete dissolution of crystals and during the
225 experiment to observe the apparition of crystals, growth and agglomeration. The video probe has a
226 field size of 720µm × 540µm and allows acquiring 25 frames per second [47].

227 **2.5.2. Optical microscopy (OM)**

228 After drying at room temperature for at least 24h, the crystals are observed under optical microscopy
229 (OM) to identify the polymorphic phases obtained and to evaluate, at the same magnification, crystals'
230 size. The optical microscope used is a Leica DM2000 LED, with different objectives with magnification
231 of 5x, 10x, 20x, 40x and 100x. The microscope is equipped with a digital camera connected to a
232 computer, which allows high-resolution image acquisition using the Leica Application Suite (LAS)
233 software.

234 **2.5.3. X-ray diffraction (XRD)**

235 XRD analyses are carried out to determine the predominant polymorph formed. The device used is a
236 Bruker D8 Advance diffractometer operating at room temperature with Kα radiation of wavelength
237 1.54060Å, a tube voltage of 40kV and a current of 40mA. Diffraction patterns are recorded using a step
238 scan method at 2 Theta values between 5° and 50° with a step size of 0.02°. Before analysis, the crystals
239 are deposited on flat-bottomed neutral supports. The diagrams obtained are then processed using the
240 DIFFRAC.EVA software and the results obtained are compared with the database to identify the
241 polymorphic phases.

242 **2.5.4. NMR analysis**

243 The quantification of ethanol in the permeate is determined by NMR. This method of analysis has the
244 advantage of not being limited by the composition. The analyses are performed with a BRUKER
245 400MHz NMR spectrometer at room temperature (298 K) with a BBFO probe for 5mm NMR tubes.

246 Ethanol shows two characteristic signals: a triplet signal at 1.19ppm, corresponding to the protons of
247 the methyl group, CH₃-, and a multiplet signal at 3.66ppm for the protons of the methylene group, -
248 CH₂-. Sodium 3-trimethylsilyl-3,3,2,2-tetradeuteriopropionate (STP) is chosen as the internal standard
249 because it is soluble in water and available at high purity. It has a simple 1H NMR spectrum consisting
250 of a single singlet of 9 protons that never overlaps with an ethanol signal [48]. The spectra are all
251 referenced to the TSP singlet peak at 0.0ppm. Samples are prepared as follows: 10mg of STP (98 atom
252 %D, Sigma-Aldrich, USA) is dissolved in 400µL of D₂O (99.9 atom %D, Sigma-Aldrich, Canada) to which
253 300µL of the sample to be analysed is then added. The NMR spectra obtained are processed using
254 BRUKER's TopSpin 4.1.0 software. To obtain reliable results, phasing and baseline correction over the
255 entire spectral range are performed manually.

256 **3. RESULTS**

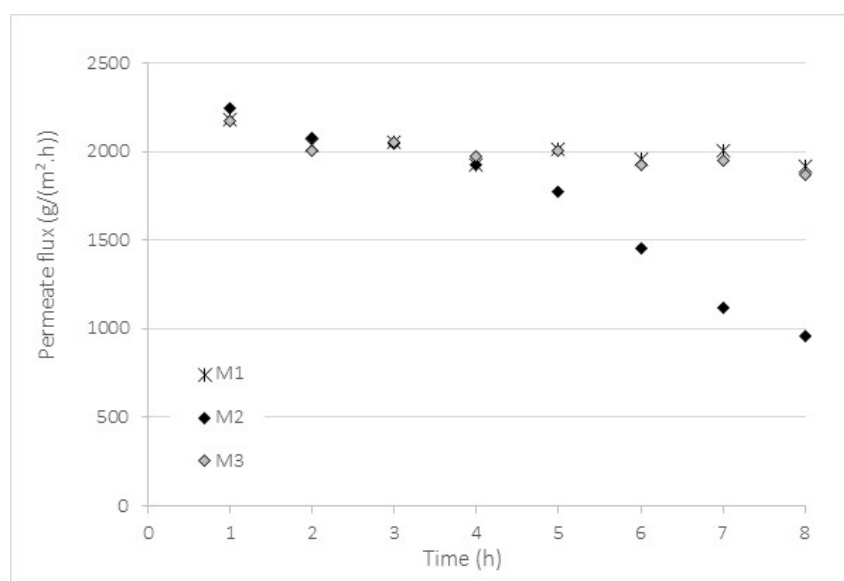
257 **3.1. Membranes ageing**

258 Before starting crystallization experiments, pervaporation with water/ethanol solution is performed
 259 to measure the separation factor and the total permeate flux of the original membranes. The
 260 separation factor and the permeate flux (cf. Table 2) are determined at 25°C, with a permeate pressure
 261 of 3mbar and an initial ethanol mass fraction of 0.122 in the solution. Both parameters are almost
 262 constant during the experiments of 5h (data not shown). The values indicated in Table 2 are thus
 263 average values measured on 5h. The separation factor and the total flux for the three membranes M1,
 264 M2 and M3 are similar, in the range of 3.6 - 4.3 and 2,300 - 2,500g/(m².h), respectively.

265 **Table 2.** References and characteristics of the membranes used

Membrane	Membrane reference	Separation factor $\beta_{\text{water/EtOH}} (-)$	Total flux (g/(m ² .h))
M1	J05-A-10	3.69	2,480
M2	J05-A-09	3.61	2,447
M3	J05-A-07	4.34	2,293

266



267

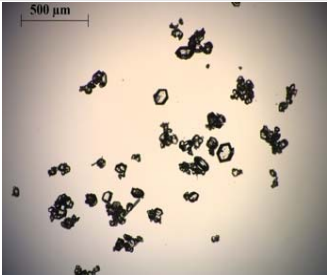
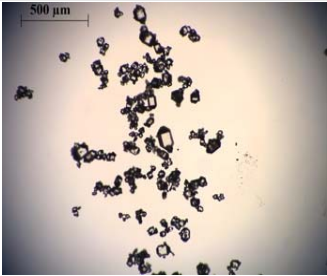
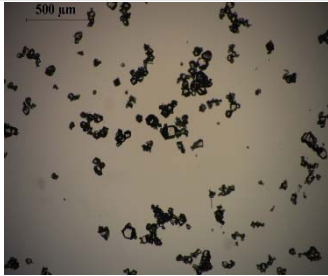
268 **Figure 4.** Permeate flux variation with time for “new” membranes, $w_{\text{EtOH,ini}} = 0.252$, $T = 25^\circ\text{C}$ and
 269 $P_{\text{permeate}} = 3\text{mbar}$

270 The performance of M1, M2 and M3 membranes are investigated with the “new” membranes, i.e. for
 271 their first use with L-glu. Experiments are carried out under the same operating conditions:
 272 $w_{\text{EtOH,ini}} = 0.252$, $T = 25^\circ\text{C}$ and $P_{\text{permeate}} = 3\text{mbar}$. Results are reported in Figure 4 and show that the
 273 permeate fluxes have the same evolution during the first 4h of experiment. The initial flux is close to
 274 2,200g/(m².h) for the three membranes and decreases after 2h, reaching 2,039g/(m².h) for M1,
 275 2,075g/(m².h) for M2 and 2,006g/(m².h) for M3. The permeate flux then remains relatively stable for
 276 M1 and M3 after 8h. However, a significant decrease is observed for M2 after 4h of experiment, from
 277 1,923g/(m².h) to 960g/(m².h). The flux decrease can be explained by different phenomena, in

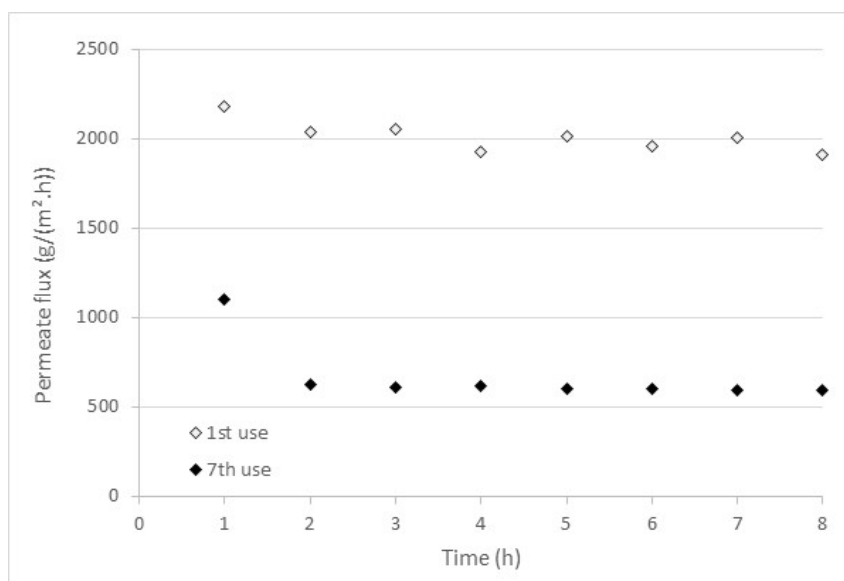
278 particular concentration polarization and/or membrane fouling. These phenomena appear more or
 279 less rapidly for the same experimental conditions. The small variation of the flux, as the one observed
 280 with M1 and M3, is only obtained during the first use of the membranes.

281 Table 3 highlights that the same polymorphic form is obtained for the three membranes: the α -form.
 282 Thus, the decrease in flux over time (observed for M2) does not influence the crystallization of one
 283 polymorph over another.

284 **Table 3.** Polymorphic forms obtained after 8h with “new” membranes

Membrane	M1	M2	M3
OM Picture (enlargement x 5)*			
Polymorphic form obtained	Mainly α	Mainly α	Mainly α

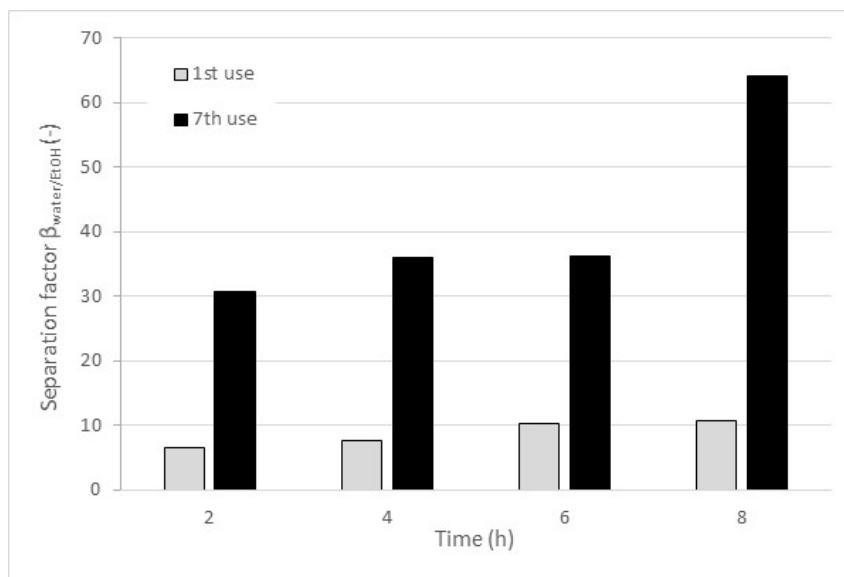
285 *OM pictures have the same scale: 500 μ m



286
 287 **Figure 5.** Permeate fluxes as a function of time for several uses of M1 membrane, $w_{EtOH,ini} = 0.252$,
 288 $T=25^{\circ}C$ and $P_{permeate} = 3mbar$

289 However, the membrane performance decreases after several uses (cf. Figure 5), despite regular
 290 regeneration of the membrane. Figure 5 shows the fluxes evolution obtained after several uses for the
 291 M1 membrane, i.e. the 1st use and the 7th use. The initial flux decreases from 2,181g/(m².h) to
 292 1,100g/(m².h) between the 1st and the 7th use. The fluxes stabilize at around 2,000g/(m².h) and
 293 600g/(m².h) after 8h, during the 1st and the 7th use, respectively. The fluxes are thus divided by 3
 294 between the 1st and the 7th use.

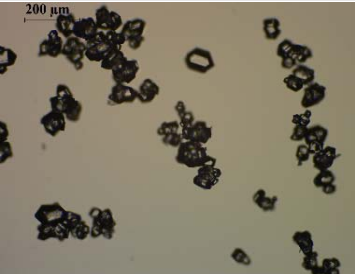

295 These results suggest membrane fouling, concentration polarization and/or surface modification of
 296 the HybSi® membranes [43,49] (by adsorption of L-glu molecules at the membrane surface and/or
 297 degradation of the selective surface by L-glu crystals). These phenomena are discussed in a following
 298 section.



299
 300 **Figure 6.** Separation factors as a function of time for the M1 membrane after the 1st use and 7th use,
 301 $w_{EtOH,ini} = 0.252$, $T=25^{\circ}C$ and $P_{permeate} = 3mbar$

302 Simultaneously with the decrease in total flux over time, a decrease in ethanol flux is observed
 303 increasing thus the water/ethanol separation factor (cf. Figure 6). After 7 uses, the membrane still
 304 maintains a high selectivity towards the water. This result is consistently observed in all subsequent
 305 experiments. Thus, although the permeate flux decreases with time, the membrane performance in
 306 terms of water/ethanol separation increases.

307 **Table 4.** Polymorphic forms mainly obtained after 1st and 7th use, M1 membrane, $w_{EtOH,ini} = 0.252$,
 308 $T=25^{\circ}C$ and $P_{permeate} = 3mbar$

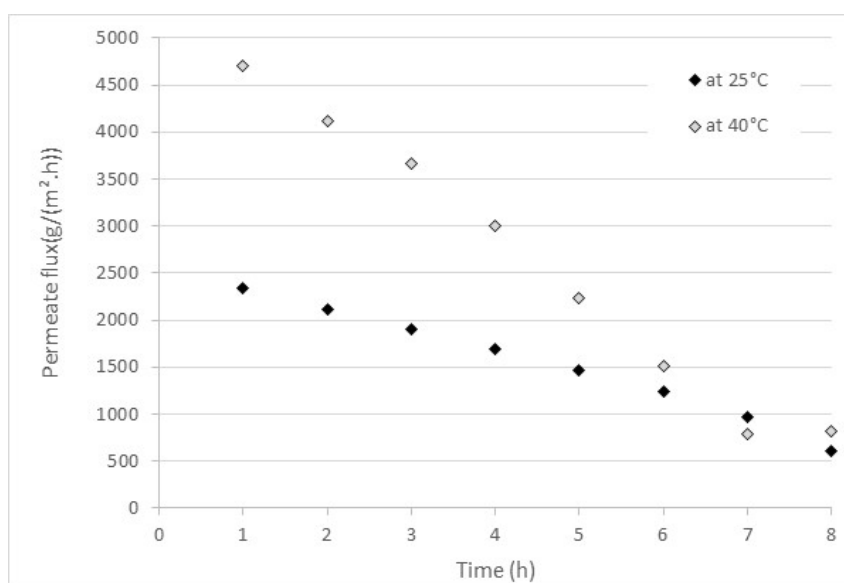
Number of use	1 st use	7 th use
Mean flux (g/(m ² .h))	2,011	669
OM Picture (enlargement x 10)*		
Polymorphic form obtained	Mainly α	Mainly α (β crystals observed by the video probe but unquantified in XRD)

309 *OM pictures have the same scale: 200μm

310 Table 4 shows that the same polymorphic form is obtained, despite the decrease of the mean flux
311 during the experiment, as confirmed by the pictures taken at the end of the 1st and the 7th experiment.
312 Hence, the polymorphic form seems to depend more on the operating conditions (initial composition
313 of the liquid phase, temperature) than on the permeate flux. However, β crystals are also observed
314 with OM after the 7th use but the amount is too small to be detected by XRD, i.e. lower than 1%wt.

315 **3.2. Temperature influence**

316 In pervaporation, the permeate flux strongly depends on the temperature. Thus, two temperatures,
317 25°C and 40°C, are investigated for $w_{\text{EtOH,ini}} = 0.122$ and $P_{\text{permeate}} = 8\text{mbar}$. The results obtained are
318 reported in Figure 7.



319

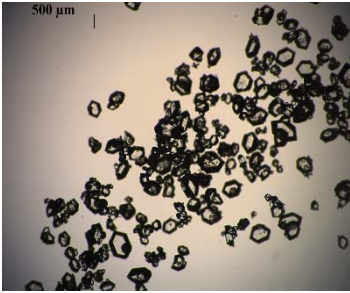
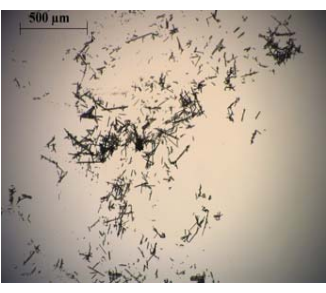
320 **Figure 7.** Total permeate flux as a function of time, $w_{\text{EtOH,ini}} = 0.122$ and $P_{\text{permeate}} = 8\text{mbar}$

321 The increase in temperature has a beneficial effect. Indeed, it leads to an increase of the initial
322 permeate flux, from 2,347g/(m²·h) to 4,703g/(m²·h). This result is consistent with what is observed for
323 pervaporation alone where the permeate flux increases with rising temperature [43,46,50].

324 However, the decrease in permeate flux is more pronounced at 40°C than at 25°C. Furthermore, after
325 7h, the permeate fluxes reach similar values, around 900g/(m²·h). This result suggests that a higher
326 permeate flux (as obtained at 40°C) leads to a higher concentration polarization and/or fouling of the
327 membrane. This phenomenon will be discussed in a following section.

328

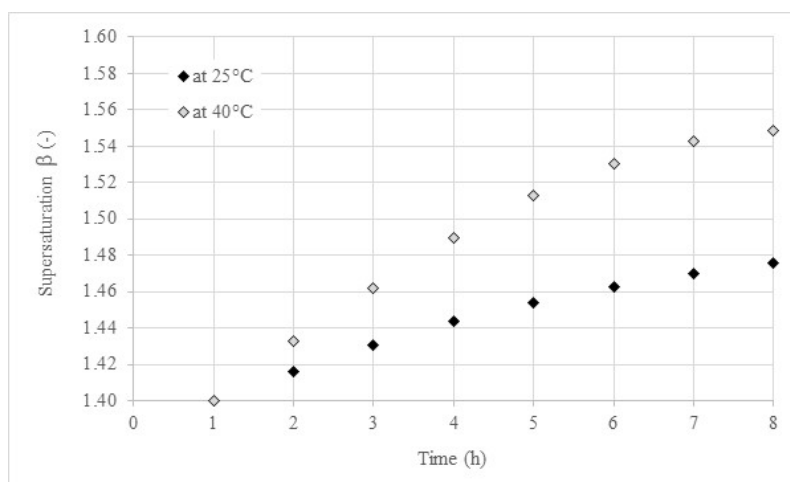
329 **Table 5.** Polymorphic forms obtained at 25°C and 40°C, $w_{EtOH,ini} = 0.122$ and $P_{permeate} = 8\text{mbar}$

Temperature	25°C	40°C
Membrane (number of use)	M2 (3 rd use)	M2 (5 th use)
Mean Flux (g/(m ² .h))	1,675	2,606
OM Picture (enlargement x 5)*		
Polymorphic form obtained	Mainly α	Mainly β

330 *OM pictures have the same scale: 500 μm

331 The temperature increase induces a significant rise of the mean flux (over 8h of experiment), from
 332 1,675g/(m².h) at 25°C to 2,606g/(m².h) at 40°C (cf. Table 5). Moreover, results highlight that at 25°C,
 333 the α -form is the main polymorphic form detected. While, the β -form is the main polymorphic form
 334 at 40°C. These observations made *in situ* by the video probe are also confirmed by OM pictures and by
 335 XRD analysis. Hence, the temperature allows producing selectively one of the polymorphic form for
 336 $w_{EtOH,ini} = 0.122$.

337



338

339 **Figure 8.** Supersaturation as function of time at the operating temperature of 25°C and 40°C,
 340 $w_{EtOH,ini} = 0.122$ and $P_{permeate} = 8\text{mbar}$

341 Figure 8 reports the evolution of the supersaturation in the reactor during the experiment. Results
 342 show that the increase of the supersaturation with time is higher at 40°C than at 25°C, which is
 343 consistent with flux results reported in Figure 7. At this step, it seems that either the temperature or
 344 the supersaturation variation during the experiment is able to control polymorphism.

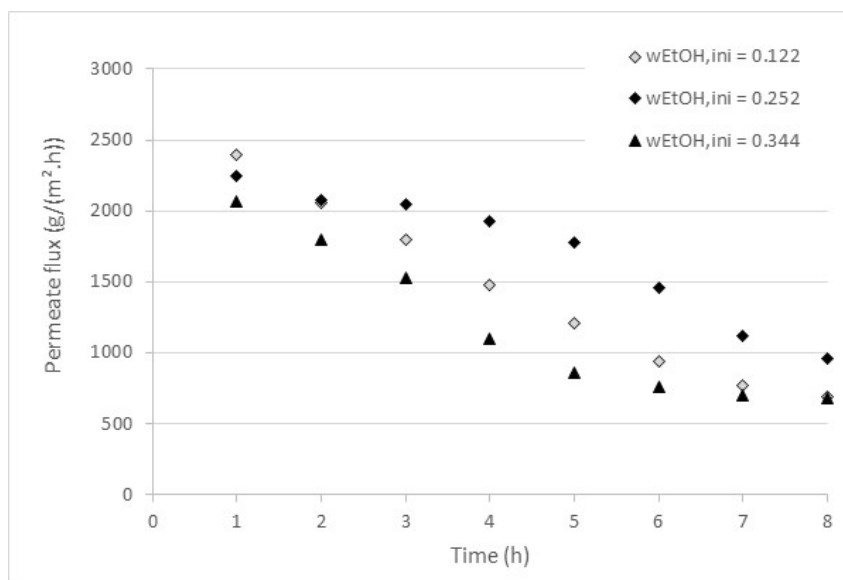
345 3.3. Influence of the initial ethanol mass fraction

346 Three mass fractions of ethanol in the initial water/ethanol mixture are studied to evaluate the
 347 influence of this parameter on the permeate flux and crystal production: 0.122, 0.252 and 0.344. In

348 the first part, the reactor temperature is set at 25°C and the pressure on the permeate side at 3mbar.
349 In the second part, the study is carried out at 40°C and the pressure is set at 8mbar.

350 3.3.1. Experiments performed at 25°C

351 At 25°C, all the experiments are performed with the M2 membrane in the following sequence: (1)
352 $w_{\text{EtOH,ini}} = 0.252$, (2) $w_{\text{EtOH,ini}} = 0.344$ and (3) $w_{\text{EtOH,ini}} = 0.122$. The results are presented in Figure 9.

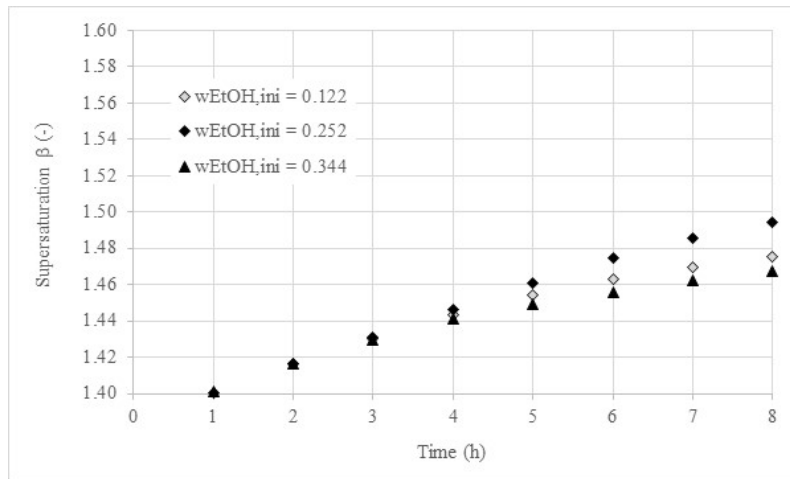


353
354 **Figure 9.** Permeate flux as function of time for various initial ethanol mass fractions at $T=25^{\circ}\text{C}$ and
355 $P_{\text{permeate}} = 3\text{mbar}$

356 Whatever the initial ethanol mass fraction, the permeate flux decreases continuously during the
357 experiment. After 1h, the flux decreases from 2,395g/(m².h) to 2,056g/(m².h) for $w_{\text{EtOH,ini}} = 0.122$; from
358 2,241g/(m².h) to 2,079g/(m².h) for $w_{\text{EtOH,ini}} = 0.252$ and from 2,070g/(m².h) to 1,798g/(m².h) for
359 $w_{\text{EtOH,ini}} = 0.344$. This flux decrease could be due to polarization concentration of ethanol and L-glu, but
360 also to the apparition of the first crystals in the reactor (confirmed by the *in situ* video), less than 2h
361 after the beginning of the experiment, those probably also be responsible in membrane fouling.

362 The permeate flux for $w_{\text{EtOH,ini}} = 0.252$ is slightly higher than the other fluxes whereas the expected
363 result is a decrease of the permeate flux with the increase of the ethanol mass fraction. This is probably
364 because the membrane has been used first for $w_{\text{EtOH,ini}} = 0.344$ and $w_{\text{EtOH,ini}} = 0.122$.

365 Despite these results, the *in situ* observation, confirmed by OM and by XRD, highlights that the main
366 polymorphic form obtained is the α -form.



367

368

369

Figure 10. Supersaturation as a function of time for various initial ethanol mass fractions at $T=25^{\circ}\text{C}$ and $P_{\text{permeate}} = 3\text{mbar}$

370

371

372

373

Results reported in Figure 10 highlight that the supersaturation do not change a lot during the experiments whatever the composition of the feed solution. The supersaturation variation during the experiments are similar to the one reported on Figure 8 at 25°C being consistent with the observation of the preferential crystallization of the α -form.

374

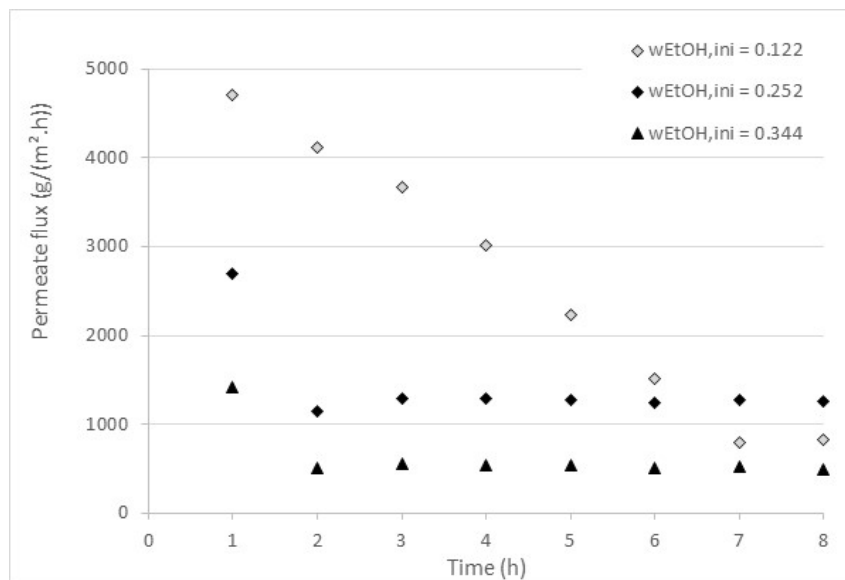
3.3.2. Experiments performed at 40°C

375

376

377

Results obtained at 40°C are reported on Figure 11. They show that, after 1h of experiment, the highest flux is reached for $w_{\text{EtOH,ini}} = 0.122$, close to $4,703\text{g}/(\text{m}^2\cdot\text{h})$ corresponding to twice the permeate flux for $w_{\text{EtOH,ini}} = 0.252$ ($2,690\text{g}/(\text{m}^2\cdot\text{h})$) and almost thrice for $w_{\text{EtOH,ini}} = 0.344$ ($1,420\text{g}/(\text{m}^2\cdot\text{h})$).



378

379

380

Figure 11. Permeate flux as function of time for various initial ethanol mass fractions at $T=40^{\circ}\text{C}$ and $P_{\text{permeate}} = 8\text{mbar}$

381

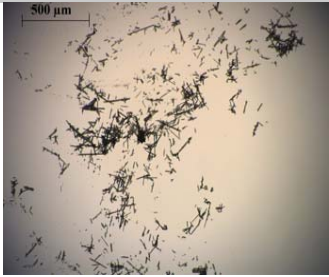


382

383

As reported previously, a significant decrease of the permeate flux is observed after 1 or 2h of experiment, especially for $w_{\text{EtOH,ini}} = 0.252$ and $w_{\text{EtOH,ini}} = 0.344$. The permeate fluxes then stabilize around $1,250\text{g}/(\text{m}^2\cdot\text{h})$ and $500\text{g}/(\text{m}^2\cdot\text{h})$, respectively. This may be the consequence of the formation of

384 a concentration polarization layer at the membrane surface. This phenomenon is well described for
 385 ultrafiltration and reverse osmosis processes [51]. Moreover, membrane fouling due to the
 386 accumulation of L-glu crystals and/or adsorption of L-glu molecules at the membrane surface can occur
 387 and induce a decrease in the permeate flux during the experiment [52]. Concentration polarization
 388 and/or fouling may be concomitant with the appearance of the first crystals, after the first hour of
 389 pervaporation, contributing more to this decrease.

390 **Table 6.** Polymorphic forms obtained at 40°C, $P_{permeate} = 8\text{mbar}$

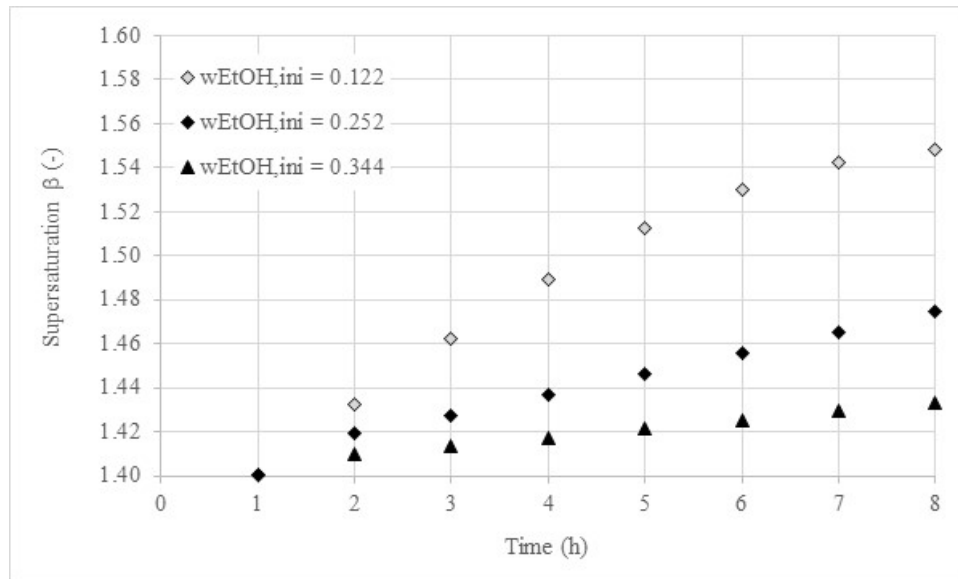
$w_{\text{EtOH,initial}}$	0.122	0.252	0.344
Membrane (number of use)	M2 (5 th use)	M2 (9 th use)	M2 (10 th use)
Mean flux (g/(m².h))	2,606	1,431	636
OM Picture (enlargement x 5)*			
Polymorphic form obtained	Mainly β Fines needles	Mixture $\alpha + \beta$ α : prismatic form β : fines needles	Mainly β Fines needles + sticks

391 *OM pictures have the same scale: 500µm

392 On the other hand, a more important decrease of the permeate flux is observed for $w_{\text{EtOH,ini}} = 0.122$. In
 393 this case, the initial permeate flux is higher and the concentration polarization and/or fouling are
 394 slower. Nevertheless, after 8h of experiment, the permeate fluxes have similar values, whatever the
 395 initial ethanol mass fraction. Table 6 reports the mean fluxes during the experiments and the
 396 polymorphic forms obtained. The β -form is the main polymorphic form for $w_{\text{EtOH,ini}} = 0.122$ and
 397 $w_{\text{EtOH,ini}} = 0.344$ (cf. Table 6). Crystals look like fine needles with a rather heterogeneous size. However,
 398 for $w_{\text{EtOH,ini}} = 0.252$, the α -form is mainly observed with a prismatic shape. These results are also
 399 confirmed by XRD.

400 The evolution of the supersaturation during experiments at 40°C are reported in Figure 12 and show
 401 that the supersaturation increases faster if the ethanol mass fraction in the feed solution is low. These
 402 results are consistent with the flux results reported on Figure 11 and with the formation of the
 403 concentration polarization layer at the membrane surface.

404 Figure 12 also confirms that whatever the supersaturation variation, the temperature seems to be the
 405 key parameter to control polymorphism.



406

407 **Figure 12.** Supersaturation as a function of time for various initial ethanol mass fractions at $T=40^{\circ}\text{C}$ and
 408 $P_{\text{permeate}} = 8\text{mbar}$

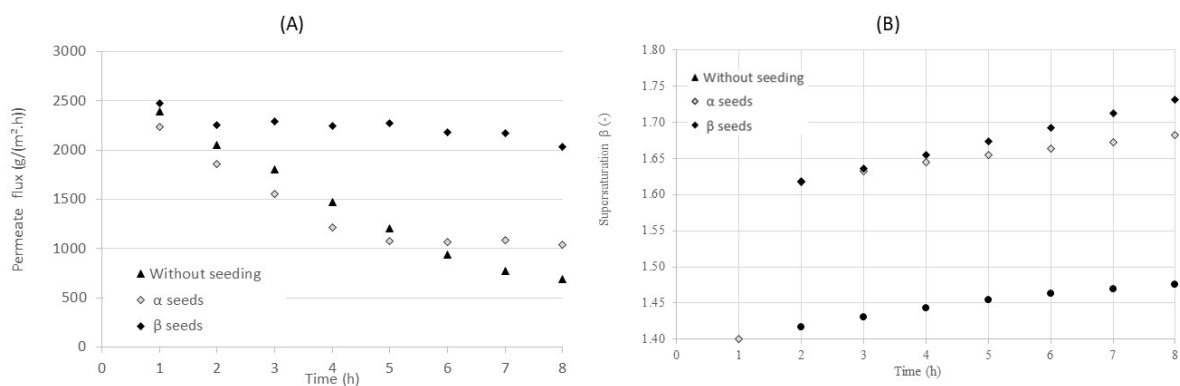
409 **3.4. Influence of seeding**

410 The addition of crystal seeds of the metastable α -form is studied. The α -form is preferred in the
 411 industry [10] and its addition as a seed should allow preferential production of this polymorphic form.
 412 The seed is added at supersaturation ($\beta = 1.4$), 1h after the beginning of the experiment. The quantity
 413 introduced corresponds to 5% of the expected theoretical final mass (cf. Table 1).

414 Seeding is expected to avoid heterogeneous nucleation by favouring the deposition of solute by growth
 415 on the seed crystals rather than the production of new nuclei. Consequently, seeding allows an
 416 increase in the size of the crystals and improves the polymorphism control [53,54].

417 In this part, the following operating parameters are fixed: $T=25^{\circ}\text{C}$ and $P_{\text{permeate}}=3\text{mbar}$. All experiments
 418 with seeding are performed with the M1 membrane while experiments without seeding are performed
 419 with the M2 membrane.

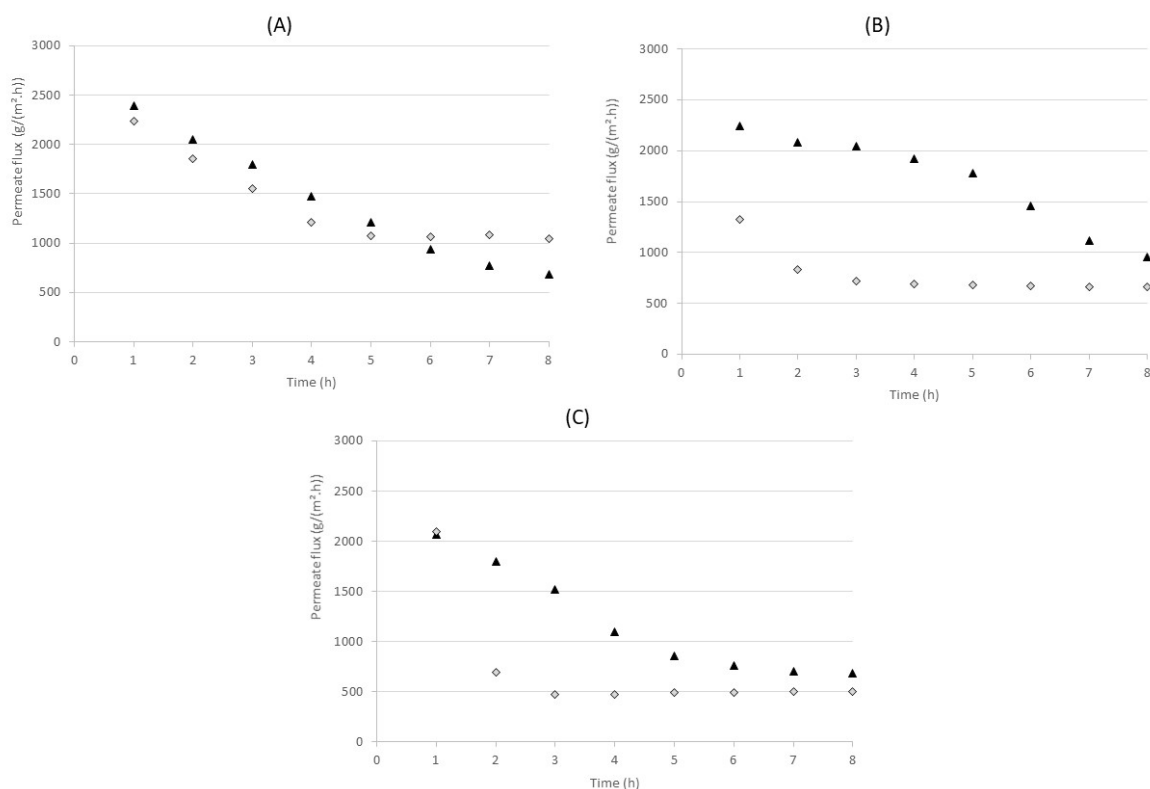
420 In addition, a test with β -seed is carried out at $T=25^{\circ}\text{C}$ for $w_{\text{EtOH},\text{ini}} = 0.122$. This is to confirm that the
 421 control of the polymorphic phase can be achieved by seeding.



422

423 **Figure 13.** Evolution of permeate fluxes (A) and supersaturation (B) with α or β seeds and without
 424 seeding for $w_{\text{EtOH},\text{ini}} = 0.122$, at 25°C and $P_{\text{permeate}} = 3\text{mbar}$

425 Figure 13 (A) shows that permeate fluxes of the experiments performed with α seeds and without
 426 seeding are close, whereas a higher and almost constant flux is achieved with the experiment seeded
 427 with β polymorph. Figure 13 (B) reports the evolution of the supersaturation during the experiment
 428 and confirms flux results: the supersaturation variation during the experiment (from 1 to 8h) is of the
 429 same order of magnitude without or with α seeding and is lower than with β seeds. Both experiments
 430 with seeding are performed with the M1 membrane: first the experiment with β seeds then with α
 431 seeds. The seed crystals are added to the solution 1h after the beginning of pervaporation. A difference
 432 is noticeable when comparing the experiments without and with β seeding since a higher and more
 433 stable flux is obtained for the experiment with β seeds. This may be due to the deposition of the L-glu
 434 by growth on the seed crystals rather than the production of new nuclei thus limiting the adsorption
 435 of L-glu on the membrane surface and hence its fouling. However, the addition of α seeds shows the
 436 lowest permeate flux. This difference could be due to the ageing of the membrane as reported
 437 previously.

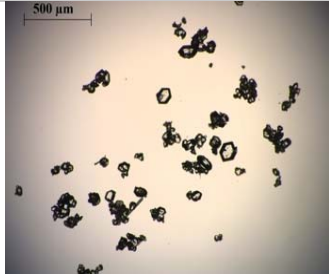
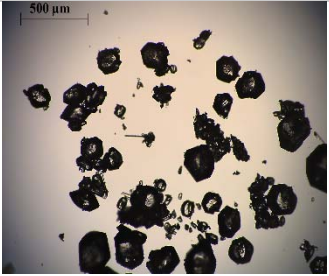
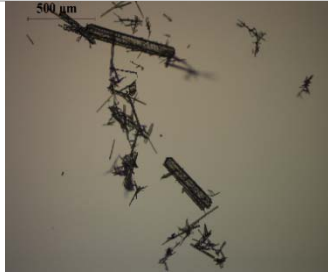


438
 439 **Figure 14.** Evolution of permeate fluxes as a function of time with α seeds (\diamond) and without seeding
 440 (\blacktriangle) for (A) $w_{EtOH,ini} = 0.122$, (B) $w_{EtOH,ini} = 0.252$, (C) $w_{EtOH,ini} = 0.344$, at 25°C and $P_{permeate} = 3\text{mbar}$

441 The addition of β seeds provides mainly crystals of β -form with a rather heterogeneous size
 442 distribution, with fine needles and rod shapes (cf. Table 7). Seeding with crystals of α -form allows
 443 keeping the α -form preferentially obtained without seeding at the same operating conditions while
 444 increasing the size of the crystals (comparison of observations made under OM). These results are
 445 confirmed by XRD.

446

447 **Table 7.** Comparison of polymorphic forms obtained with or without seeding for $w_{\text{EtOH},\text{ini}} = 0.122$, at
 448 25°C and $P_{\text{permeate}} = 8\text{mbar}$


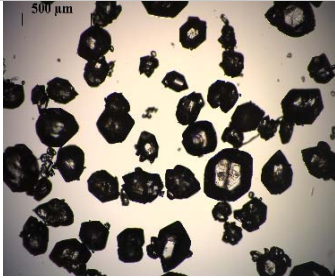
	No seeding	α seeds	β seeds
Membrane (number of use)	M2 (3 rd use)	M1 (5 th use)	M1 (4 th use)
OM Picture (enlargement x 5)*			
Polymorphic form obtained	Mainly α	Mainly α	Mainly β

449 *OM pictures have the same scale: 500 μm

450 The experiments are then carried out with α seeds or without seeding for several initial ethanol mass
 451 fractions. The results are presented in Figure 14 and show that the permeate flux decreases after the
 452 addition of the seed. However, this decrease is more important for $w_{\text{EtOH},\text{ini}} = 0.252$ and $w_{\text{EtOH},\text{ini}} = 0.344$.
 453 For $w_{\text{EtOH},\text{ini}} = 0.122$, the permeate fluxes with or without seeding are very close whereas a decrease is
 454 expected, as reported for the two other ethanol mass fractions. This phenomenon could be due to the
 455 membrane M2 aging for $w_{\text{EtOH},\text{ini}} = 0.252$ and $w_{\text{EtOH},\text{ini}} = 0.344$, i.e. with or without seeding; while two
 456 membranes (M1 and M2) are used which could explain the flux difference observed with the two other
 457 ethanol mass fractions.

458 The main results for each ethanol mass fraction with or without seeding are shown in Tables 7, 8 and
 459 9.

460 **Table 8.** Comparison of polymorphic forms obtained with α seeds or without seeding for
 461 $w_{\text{EtOH},\text{ini}} = 0.252$, at 25°C and $P_{\text{permeate}} = 8\text{mbar}$


	No seeding	Seeding
Membrane (number of use)	M2 (1 st use)	M2 (6 th use)
OM Picture (enlargement x 5)*		
Polymorphic form obtained	Mainly α	Mainly α

462 *OM pictures have the same scale: 500 μm

463

464

465 **Table 9.** Comparison of polymorphic forms obtained with α seeds or without seeding for $w_{\text{EtOH},\text{ini}} = 0.344$,
 466 at 25°C and $P_{\text{permeate}} = 8\text{mbar}$

	No seeding	Seeding
Membrane (number of use)	M2 (2 nd use)	M2 (7 th use)
OM Picture (enlargement x 5)*	Not enough of crystals	
Polymorphic form obtained	/	Mainly α

467 *OM pictures have the same scale: $500\mu\text{m}$

468 As shown in Table 7 to Table 9, the metastable form is mainly obtained at 25°C whatever the ethanol
 469 mass fraction, with or without seeding. A significant increase in crystal size is observed after seeding.
 470 On the other hand, in the experiments achieved with seeding, traces of β -form are detected by the *in*
 471 *situ* video probe and some crystals are observed under OM. These results are also confirmed by XRD.

472 4. DISCUSSION

473 The permeate flux variations over time and after several uses, the adsorption of L-glu on the
 474 membrane surface and the influence of the operating parameters on the polymorphic forms obtained
 475 are successively discussed below.

476 4.1. Change of the permeate flux

477 During the first use of the HybSi[®] membrane for crystallization using pervaporation, the permeate flux
 478 remains constant over 8h, with only a slight decrease of the flux with time, except in the case of the
 479 M2 membrane (cf. Figure 4). Indeed, important decrease of the permeate flux with time is observed
 480 after the first use. Similar decrease in permeate flux is reported in the literature for the organic solvent
 481 dehydration by pervaporation [43,46]. Nevertheless, the decrease reported is not as important and it
 482 is difficult to compare it to our results, where pervaporation is associated to crystallization.

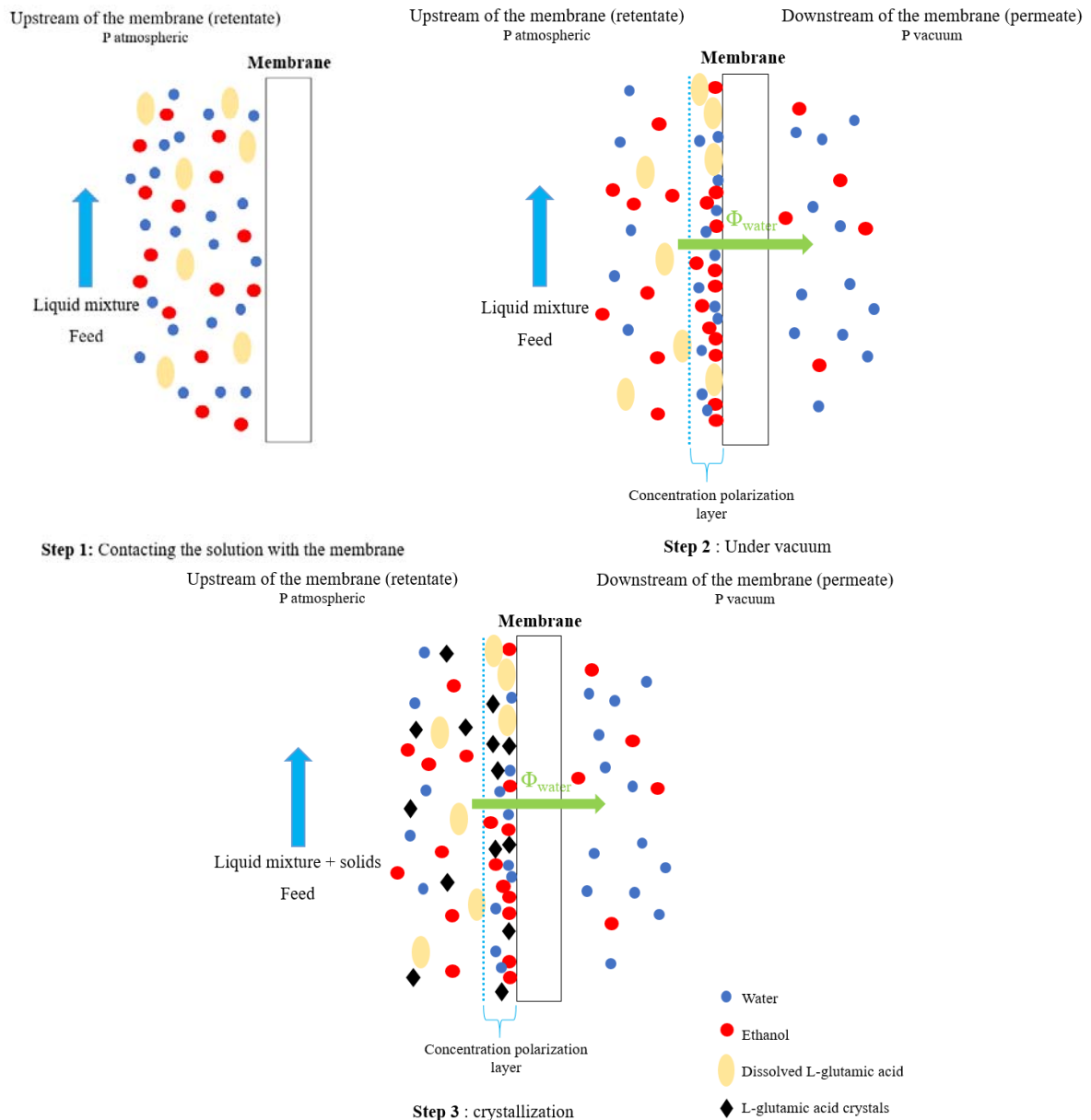
483 During pervaporation of water/ethanol solutions, the permeate flux is almost constant during 5h,
 484 whatever the ethanol mass fraction studied. This observation means that ethanol is not the main
 485 responsible for the decrease observed in our pervaporation/crystallization experiments. Hence, L-glu
 486 seems to have a direct influence on the observed permeate flux decrease.

487 Therefore, the adsorption of L-glu and the formation of crystals at the membrane surface could be
 488 responsible for the progressive decrease of water permeation through the membrane (cf. Figure 15).

489 Thus, it is assumed that a series of events, as described below, contributes to this phenomenon:

- 490 i. The preferential diffusion of water through the hydrophilic membrane contributes to create a
 491 concentration polarization layer of ethanol and dissolved L-glu at the membrane surface. The
 492 formation of this boundary layer could explain the stable permeate flux after 1 or 2h, according
 493 to the experimental conditions.

- 494 ii. The tangential flow does not provide sufficient shear stress to "sweep" the accumulated
 495 molecules and/or crystals along the membrane surface, even under turbulent conditions.
 496 iii. In parallel, the crystals' formation near and at the membrane surface, which is the place where
 497 the supersaturation is the most important, contributes to decrease the permeate flux with
 498 time by adding a surface fouling phenomenon. In addition, the evaporation of water through
 499 the membrane produces a local cooling leading to faster crystallization at the surface and near
 500 the membrane.
 501 When these phenomena are not reversible, the membrane regeneration is not sufficient to restore
 502 the initial flux and the membrane performance decreases with the number of uses.



503

504

505

506

Figure 15. Illustration of concentration polarization and fouling during crystallization using pervaporation

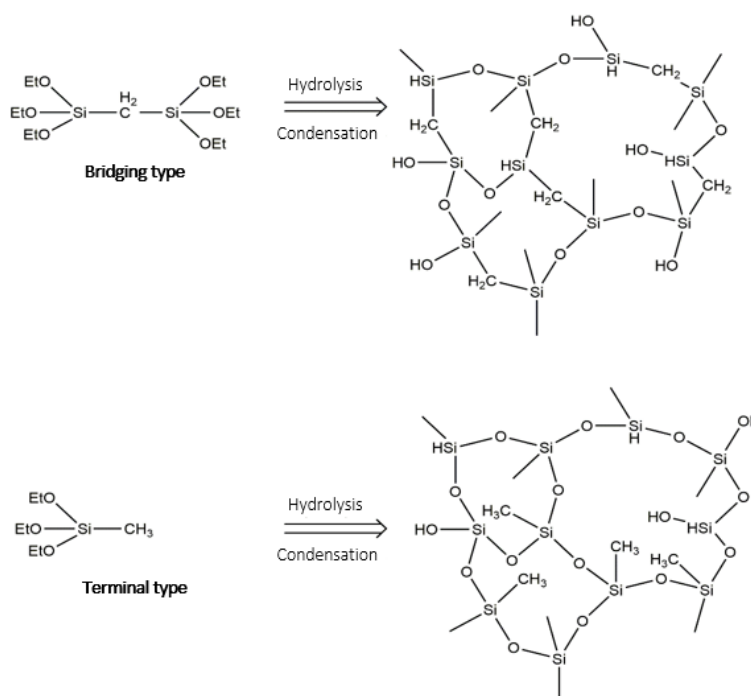
507 **4.2. Adsorption of L-glutamic acid at the HybSi® membrane surface**

508 As reported in the seeding part, a decrease in the permeate flux is observed with time during the
509 experiments but also with repeated uses of the HybSi® membrane. The adsorption of L-glu at the
510 membrane surface could be an explanation for the fouling phenomenon.

511 L-glu is available under several chemical forms according to the pH of the solution: a cationic form at
512 $\text{pH} \leq 2.19$, an anionic form at $\text{pH} \geq 4.25$, and a zwitterionic form between 2.19 and 4.25 [55].

513 In addition, BTESM is a precursor belonging to the organoalkoxysilane family. According to the position
514 of the organic groups (CH_2 and CH_3) in the organosilica networks, BTSEM has two configurations: (1)
515 the bridging position type ($-\text{Si}-\text{CH}_2-\text{Si}-$), (2) the terminal position ($-\text{Si}-\text{CH}_3$) [56]. Both types are reported
516 in Figure 16. Organic groups are much considered as spacers between silica atoms of the structure of
517 the organosilica networks. If the organic groups are in a terminal position, they don't act like spacers
518 and can easily fill the pores created by the silica structure as shown in Figure 16 [42,57].

519



520

521 **Figure 16.** Possible configuration of BTESM: bridging and terminal position and their derived networks
522 [56]

523 There are free $-\text{OH}$ groups on the surface of the membrane, responsible for its hydrophilic nature.
524 These groups are also able to interact with L-glu molecules by making hydrogen bonds with the $-\text{COOH}$
525 groups. This phenomenon has been previously described for the dehydration of ethyl acrylate from
526 acrylic acid using a PVA membrane [49]. The stability study of these membranes has been performed
527 by comparing results obtained on a new membrane and an artificially aged membrane. The analysis,
528 achieved by IR spectroscopy, showed changes after one month of continuous pervaporation. The $-\text{OH}$
529 groups decreased while a significant increase in the $\text{C}=\text{O}$ groups have been detected. The authors
530 assumed that it could be due to a chemical reaction between the $-\text{OH}$ group of the membrane and
531 acrylic acid [49].

532 Hence, adsorption of L-glu molecules on the membrane surface can lead to a significant decrease in
 533 the permeate flux during the experiment. Moreover, the dissolved L-glu molecules can promote
 534 heterogeneous nucleation at the membrane surface, as the solution is locally highly supersaturated.
 535 These nuclei could also extend on the membrane surface and thus contribute to a further decrease in
 536 the flux. Hence, a decrease of the membrane performance, due to degradation of the selective fine
 537 layer of HybSi[®], is expected after a certain number of use (after around 12 uses for the M2 membrane,
 538 fluxes and separation factors have been divided by 2 (data not shown)).

539 **4.3. Influence of operating parameter on the polymorphic form obtained**

540 Table 10 summarize the polymorphic forms obtained according to the operating conditions for two
 541 ethanol mass fractions.

542 **Table 10.** Summary of the polymorphic forms obtained for $w_{\text{EtOH},ini} = 0.122$

Operating parameter	Polymorphic form	
Permeate pressure (mbar)	3	Mainly α
	8	Mainly α
Temperature (°C)	25	Mainly α
	40	Mainly β
Seeding at 25°C	-	Mainly α
	α	Mainly α
	β	Mainly β
Seeding at 40°C	-	Mainly β
	α	Mixture of α and β but mainly β

543 Table 10 highlights that temperature has a significant influence on the selection of the polymorphic
 544 form for the ethanol mass fraction of 0.122. Indeed, the α -form is the main polymorphic form
 545 produced at 25°C while it is the β -form at 40°C. However, the increase of the permeate pressure does
 546 not influence the polymorphic form for $w_{\text{EtOH},ini} = 0.122$ (cf. Table 10).

547 In contrast, a mixture of both polymorphs, mainly with the α -form is observed at 40°C for
 548 $w_{\text{EtOH},ini} = 0.252$, (cf. Table 11). At the beginning of the experiment, the α -form is observed and then a
 549 phase transition occurs. At high temperatures, the thermodynamically stable β -form tends to
 550 crystallize preferentially.

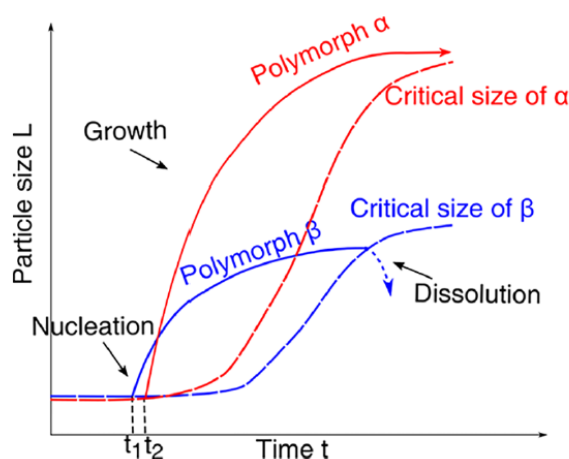
551 **Table 11.** Summary of the polymorphic forms obtained for $w_{\text{EtOH},ini} = 0.252$, at $P_{\text{permeate}} = 3\text{mbar}$

Operating parameters	Polymorphic form obtained	
Seeding at 25°C	-	Mainly α
	α	Mainly α
Seeding at 40°C	-	Mixture of α and β but mainly α
	α	Mixture of α and β but mainly α

552 These observations are consistent with those reported in the literature [58,59]. Indeed, one of the key
 553 parameters to control the crystallization of a polymorphic form on another seems to be the
 554 temperature. According to the work of Tahri et al., at low temperature ($\approx 5^\circ\text{C}$) and low supersaturation,

555 the nucleation and growth of polymorph α are faster and a preferential crystallization of this
556 polymorph is observed [60]. In this work, metastable crystals are spontaneously obtained at 25°C for
557 $w_{\text{EtOH,ini}} = 0.122$ and $w_{\text{EtOH,ini}} = 0.252$, and at 40°C for $w_{\text{EtOH,ini}} = 0.252$. The addition of antisolvent in the
558 initial solution moves the nucleation area of the α -form forward. This behaviour follows the Ostwald
559 rules of stages which suggests that a chemical system does not tend the most stable state, but rather
560 tends towards the closest metastable state [61].

561 Tahri et al. suggested a kinetic explanation of the Ostwald rules of stages, based on an original ripening
562 mechanism occurring between polymorphs clusters [60]. According to the authors, in the first step of
563 the crystallization, at the nanometric scale, both polymorphs nucleate. Nevertheless, because of the
564 rapid growth of the metastable phase clusters consuming the supersaturation, the slow-growing
565 clusters of the stable polymorph become undersaturated and dissolve (cf. Figure 17). Therefore, if the
566 difference in growth kinetics between the polymorphs is high while their equilibrium concentrations
567 are close, the Gibbs-Thomson effect may allow the preferential crystallization of the metastable
568 polymorph at the expense of the stable polymorph, leading to the macroscopic observation of Ostwald
569 rules of stages [60].



570
571 **Figure 17.** Competition between both polymorphs of L-glutamic acid, leading to the production of the
572 metastable α polymorph [60]

573 At high temperatures ($\geq 40^\circ\text{C}$) and low supersaturation, the nucleation rate of the α -form is low while
574 the growth rate of the β -form is more important. In the competition between the two polymorphs,
575 β nuclei sizes manage then to remain over the critical size all along the nucleation process which
576 justifies the prevalence of the β -form [62].

577 Of all the different parameters involved in the crystallization process of polymorphs, the suggested
578 ripening mechanism seems to have an important role. Considering this mechanism between
579 polymorphs could be useful for the control of the polymorphic phase obtained in industrial processes
580 or for their screening.

581 5. CONCLUSION

582 This study describes the pervaporation process applied to the crystallization of L-glu. The purpose is to
583 determine the experimental parameters allowing the control of the crystals' final properties (size and
584 polymorphic form) and to identify the limiting parameters of the process. It is found that temperature

585 is a major parameter that controls the membrane's selectivity as well as the polymorphic phases
586 produced. Moreover, a significant decrease in permeate flux as a function of time is obtained for
587 experimental conditions where the initial flux is high. Stabilization of the flux after 1h or 2h of
588 pervaporation is observed, for lower initial flux values. The permeate flux also decreases with the
589 repeated use of the same membrane, the regeneration does not allow to find the initial value of the
590 flux. The achievement of a stabilized flux after 1h or 2h of pervaporation/crystallization can be
591 explained by the formation of a boundary layer on the surface of the membrane. The decrease in
592 permeate flux is the consequence of several phenomena: the concentration polarization of ethanol
593 and L-glu acid molecules and membrane fouling as result of the adsorption of dissolved L-glu acid
594 molecules and L-glu crystallization on the membrane surface (where supersaturation is locally very
595 high). Fouling contributes after several uses, to reduce the performance of the membrane and
596 therefore the process.
597 Results obtained show the feasibility of the pervaporation process applied to the crystallization of L-
598 glu. It is found that the polymorph formed does not directly depend on the permeate flux but more on
599 the operating conditions and particularly on the temperature and the mass fraction of ethanol in the
600 initial water/ethanol mixture.

601 **LIST OF SYMBOLS AND ABBREVIATIONS**

602 ***Abbreviations***

603 BTESE: bis(triethoxysilyl)ethane
604 BTESM: bis(triethoxysilyl)methane
605 CSD: Crystal Size Distribution
606 D₂O: Deuterium oxide
607 M1, M2, M3: membrane 1, 2, 3
608 NMR: Nuclear Magnetic Resonance
609 OM: Optical Microscopy
610 SEM: Scanning Electron Microscopy
611 STP: Sodium 3-trimethylsilyl-3,3,2,2-tetradeuteriopropionate
612 XRD: X-Ray Diffraction

613 ***Symbols***

614 α : Metastable polymorph of L-glutamic acid
615 β : Stable polymorph of L-glutamic acid
616 $\beta_{\text{water/EtOH}}$: water/ethanol separation factor (-)
617 J_i : Partial flux of compound i (kg/(m².h))
618 J_{tot} : Total flux of permeate (kg/(m².h))
619 m_p : Mass of permeate recovered in the trap (g)
620 Re: Reynolds number
621 S: Effective membrane area (m²)
622 t: Time (h)
623 w_i^p : Mass fraction of compound i in the permeate (-)

624 ***Index and expositis***

625 EtOH : Ethanol

626 f: feed
627 i: Chemical species considered (water or ethanol)
628 ini: Initial
629 L-glu : Acide L-glutamique
630 p : Permeate
631 tot : Total
632 w : Water
633
634
635

636 **ACKNOWLEDGEMENTS**

637 We would like to thank Ruben Vera for the X-ray diffraction measurements (Centre de Diffractométrie
638 Henri Longchambon, Université Lyon 1, Villeurbanne - France) and Emmanuel Chefdeville for the NMR
639 analysis (Centre Commun de RMN, Université Lyon 1, Villeurbanne - France).

640 **BIBLIOGRAPHY**

- 641 [1] B.Y. Shekunov, P. York, Crystallization processes in pharmaceutical technology and drug delivery
642 design, *Journal of Crystal Growth*. 211 (2000) 122–136. [https://doi.org/10.1016/S0022-](https://doi.org/10.1016/S0022-0248(99)00819-2)
643 [0248\(99\)00819-2](https://doi.org/10.1016/S0022-0248(99)00819-2).
- 644 [2] T.-T.C. Lai, S. Ferguson, L. Palmer, B.L. Trout, A.S. Myerson, Continuous Crystallization and
645 Polymorph Dynamics in the L-Glutamic Acid System, *Org. Process Res. Dev.* 18 (2014) 1382–1390.
646 <https://doi.org/10.1021/op500171n>.
- 647 [3] J. Orehek, D. Teslić, B. Likozar, Continuous Crystallization Processes in Pharmaceutical
648 Manufacturing: A Review, *Org. Process Res. Dev.* 25 (2021) 16–42.
649 <https://doi.org/10.1021/acs.oprd.0c00398>.
- 650 [4] M. Michaud, D. Mangin, C. Charcosset, E. Chabanon, Dense Membrane Crystallization in Gas–
651 Liquid Systems: Key Parameters Influencing Fouling, *Ind. Eng. Chem. Res.* 58 (2019) 20134–
652 20146. <https://doi.org/10.1021/acs.iecr.9b03907>.
- 653 [5] C. Charcosset, Membrane processes in biotechnology: An overview, *Biotechnology Advances*. 24
654 (2006) 482–492. <https://doi.org/10.1016/j.biotechadv.2006.03.002>.
- 655 [6] C. Charcosset, R. Kieffer, D. Mangin, F. Puel, Coupling between Membrane Processes and
656 Crystallization Operations, *Industrial & Engineering Chemistry Research*. 49 (2010) 5489–5495.
657 <https://doi.org/10.1021/ie901824x>.
- 658 [7] E. Drioli, G. Di Profio, E. Curcio, Progress in membrane crystallization, *Current Opinion in Chemical*
659 *Engineering*. 1 (2012) 178–182. <https://doi.org/10.1016/j.coche.2012.03.005>.
- 660 [8] G. Di Profio, S. Tucci, E. Curcio, E. Drioli, Controlling Polymorphism with Membrane-Based
661 Crystallizers: Application to Form I and II of Paracetamol, *Chemistry of Materials*. 19 (2007) 2386–
662 2388. <https://doi.org/10.1021/cm0701005>.
- 663 [9] G. Di Profio, S. Tucci, E. Curcio, E. Drioli, Selective Glycine Polymorph Crystallization by Using
664 Microporous Membranes, *Crystal Growth & Design*. 7 (2007) 526–530.
665 <https://doi.org/10.1021/cg0605990>.
- 666 [10] G. Di Profio, E. Curcio, S. Ferraro, C. Stabile, E. Drioli, Effect of Supersaturation Control and
667 Heterogeneous Nucleation on Porous Membrane Surfaces in the Crystallization of L-Glutamic
668 Acid Polymorphs, *Crystal Growth & Design*. 9 (2009) 2179–2186.
669 <https://doi.org/10.1021/cg800838b>.

- 670 [11] G. Di Profio, C. Stabile, A. Caridi, E. Curcio, E. Drioli, Antisolvent membrane crystallization of
671 pharmaceutical compounds, *Journal of Pharmaceutical Sciences*. 98 (2009) 4902–4913.
672 <https://doi.org/10.1002/jps.21785>.
- 673 [12] G. Di Profio, M.T. Reijonen, R. Caliandro, A. Guagliardi, E. Curcio, E. Drioli, Insights into the
674 polymorphism of glycine: membrane crystallization in an electric field, *Physical Chemistry
675 Chemical Physics*. 15 (2013) 9271. <https://doi.org/10.1039/c3cp50664a>.
- 676 [13] E. Drioli, G. Di Profio, E. Curcio, *Membrane-assisted crystallization technology*, World Scientific,
677 London ; Hackensack, NJ, 2015.
- 678 [14] G. Di Profio, V. Grosso, A. Caridi, R. Caliandro, A. Guagliardi, G. Chita, E. Curcio, E. Drioli, Direct
679 production of carbamazepine–saccharin cocrystals from water/ethanol solvent mixtures by
680 membrane-based crystallization technology, *CrystEngComm*. 13 (2011) 5670.
681 <https://doi.org/10.1039/c1ce05410d>.
- 682 [15] A. Jonquière, R. Clément, P. Lochon, J. Néel, M. Dresch, B. Chrétien, Industrial state-of-the-art
683 of pervaporation and vapour permeation in the western countries, *Journal of Membrane Science*.
684 206 (2002) 87–117. [https://doi.org/10.1016/S0376-7388\(01\)00768-2](https://doi.org/10.1016/S0376-7388(01)00768-2).
- 685 [16] C.S. Slater, M.J. Savelski, T.M. Moroz, M.J. Raymond, Pervaporation as a green drying process for
686 tetrahydrofuran recovery in pharmaceutical synthesis, *Green Chemistry Letters and Reviews*. 5
687 (2012) 55–64. <https://doi.org/10.1080/17518253.2011.578590>.
- 688 [17] D. Shah, K. Kissick, A. Ghorpade, R. Hannah, D. Bhattacharyya, Pervaporation of alcohol–water
689 and dimethylformamide–water mixtures using hydrophilic zeolite NaA membranes: mechanisms
690 and experimental results, *Journal of Membrane Science*. 179 (2000) 185–205.
691 [https://doi.org/10.1016/S0376-7388\(00\)00515-9](https://doi.org/10.1016/S0376-7388(00)00515-9).
- 692 [18] C. Yu, Y. Liu, G. Chen, X. Gu, W. Xing, Pretreatment of Isopropanol Solution from Pharmaceutical
693 Industry and Pervaporation Dehydration by NaA Zeolite Membranes, *Chinese Journal of Chemical
694 Engineering*. 19 (2011) 904–910. [https://doi.org/10.1016/S1004-9541\(11\)60071-2](https://doi.org/10.1016/S1004-9541(11)60071-2).
- 695 [19] D. Shah, D. Bhattacharyya, A. Ghorpade, W. Mangum, Pervaporation of pharmaceutical waste
696 streams and synthetic mixtures using water selective membranes, *Environmental Progress*. 18
697 (1999) 21–29. <https://doi.org/10.1002/ep.670180116>.
- 698 [20] R.W. Baker, *Membrane technology and applications*, 2nd ed, J. Wiley, Chichester ; New York,
699 2004.
- 700 [21] G. Liu, W. Jin, Pervaporation membrane materials: Recent trends and perspectives, *Journal of
701 Membrane Science*. 636 (2021) 119557. <https://doi.org/10.1016/j.memsci.2021.119557>.
- 702 [22] X. Cheng, F. Pan, M. Wang, W. Li, Y. Song, G. Liu, H. Yang, B. Gao, H. Wu, Z. Jiang, Hybrid
703 membranes for pervaporation separations, *Journal of Membrane Science*. 541 (2017) 329–346.
704 <https://doi.org/10.1016/j.memsci.2017.07.009>.
- 705 [23] P.A. Kober, *Pervaporation, Persiltation and Percrystallization*, *J. Am. Chem. Soc.* 39 (1917) 944–
706 948. <https://doi.org/10.1021/ja02250a011>.
- 707 [24] K.W. Böddeker, I.L. Gatfield, J. Jähnig, C. Schorm, Pervaporation at the vapor pressure limit:
708 Vanillin, *Journal of Membrane Science*. 137 (1997) 155–158. [https://doi.org/10.1016/S0376-7388\(97\)00187-7](https://doi.org/10.1016/S0376-7388(97)00187-7).
- 709 [25] X. Zhang, C. Li, X. Hao, X. Feng, H. Zhang, H. Hou, G. Liang, Recovering phenol as high purity
710 crystals from dilute aqueous solutions by pervaporation, *Chemical Engineering Science*. 108
711 (2014) 183–187. <https://doi.org/10.1016/j.ces.2014.01.011>.
- 712 [26] C. Li, X. Zhang, X. Hao, X. Feng, X. Pang, H. Zhang, Thermodynamic and mechanistic studies on
713 recovering phenol crystals from dilute aqueous solutions using pervaporation–crystallization
714 coupling (PVCC) system, *Chemical Engineering Science*. 127 (2015) 106–114.
715 <https://doi.org/10.1016/j.ces.2015.01.039>.
- 716 [27] W. Zeng, B. Li, H. Li, H. Jin, D. Wu, Y. Li, A pervaporation-crystallization (PC) process for
717 simultaneous recovery of ethanol and sodium pyruvate from waste centrifugal mother liquid,
718 *Journal of Membrane Science*. 619 (2021) 118749.
719 <https://doi.org/10.1016/j.memsci.2020.118749>.
- 720

- 721 [28] M. Gryta, Fouling in direct contact membrane distillation process, *Journal of Membrane Science*.
722 325 (2008) 383–394. <https://doi.org/10.1016/j.memsci.2008.08.001>.
- 723 [29] R. Kieffer, D. Mangin, F. Puel, C. Charcosset, Precipitation of barium sulphate in a hollow fiber
724 membrane contactor, Part I: Investigation of particulate fouling, *Chemical Engineering Science*.
725 64 (2009) 1759–1767. <https://doi.org/10.1016/j.ces.2009.01.011>.
- 726 [30] X. Zhang, L. Fan, F.A. Roddick, Effect of feedwater pre-treatment using UV/H₂O₂ for mitigating
727 the fouling of a ceramic MF membrane caused by soluble algal organic matter, *Journal of*
728 *Membrane Science*. 493 (2015) 683–689. <https://doi.org/10.1016/j.memsci.2015.07.024>.
- 729 [31] B. Ma, W. Xue, Y. Bai, R. Liu, W. Chen, H. Liu, J. Qu, Enhanced alleviation of ultrafiltration
730 membrane fouling by regulating cake layer thickness with pre-coagulation during drinking water
731 treatment, *Journal of Membrane Science*. 596 (2020) 117732.
732 <https://doi.org/10.1016/j.memsci.2019.117732>.
- 733 [32] R. Fabris, E.K. Lee, C.W.K. Chow, V. Chen, M. Drikas, Pre-treatments to reduce fouling of low
734 pressure micro-filtration (MF) membranes, *Journal of Membrane Science*. 289 (2007) 231–240.
735 <https://doi.org/10.1016/j.memsci.2006.12.003>.
- 736 [33] L.L.A. Koh, H.T.H. Nguyen, J. Chandrapala, B. Zisu, M. Ashokkumar, S.E. Kentish, The use of
737 ultrasonic feed pre-treatment to reduce membrane fouling in whey ultrafiltration, *Journal of*
738 *Membrane Science*. 453 (2014) 230–239. <https://doi.org/10.1016/j.memsci.2013.11.006>.
- 739 [34] A.S. Al-Amoudi, Factors affecting natural organic matter (NOM) and scaling fouling in NF
740 membranes: A review, *Desalination*. 259 (2010) 1–10.
741 <https://doi.org/10.1016/j.desal.2010.04.003>.
- 742 [35] E. Gwon, M. Yu, H. Oh, Y. Ylee, Fouling characteristics of NF and RO operated for removal of
743 dissolved matter from groundwater, *Water Research*. 37 (2003) 2989–2997.
744 [https://doi.org/10.1016/S0043-1354\(02\)00563-8](https://doi.org/10.1016/S0043-1354(02)00563-8).
- 745 [36] R. Sheikholeslami, S. Zhou, Performance of RO membranes in silica bearing waters, *Desalination*.
746 132 (2000) 337–344. [https://doi.org/10.1016/S0011-9164\(00\)00169-7](https://doi.org/10.1016/S0011-9164(00)00169-7).
- 747 [37] Y. Zhou, J. Wang, T. Wang, N. Wang, Y. Xiao, S. Zong, X. Huang, H. Hao, Self-Assembly of
748 Monodispersed Carnosine Spherical Crystals in a Reverse Antisolvent Crystallization Process,
749 *Crystal Growth & Design*. 19 (2019) 2695–2705. <https://doi.org/10.1021/acs.cgd.8b01818>.
- 750 [38] L. Martínez-Díez, M.I. Vázquez-González, Temperature polarization in mass transport through
751 hydrophobic porous membranes, *AIChE J.* 42 (1996) 1844–1852.
752 <https://doi.org/10.1002/aic.690420706>.
- 753 [39] I.L. Borisov, A. Kujawska, K. Knozowska, V.V. Volkov, W. Kujawski, Influence of feed flow rate,
754 temperature and feed concentration on concentration polarization effects during separation of
755 water-methyl acetate solutions with high permeable hydrophobic pervaporation PDMS
756 membrane, *Journal of Membrane Science*. 564 (2018) 1–9.
757 <https://doi.org/10.1016/j.memsci.2018.07.001>.
- 758 [40] B. Ravindra Babu, N.K. Rastogi, K.S.M.S. Raghavarao, Concentration and temperature
759 polarization effects during osmotic membrane distillation, *Journal of Membrane Science*. 322
760 (2008) 146–153. <https://doi.org/10.1016/j.memsci.2008.05.041>.
- 761 [41] H.L. Castricum, R. Kreiter, H.M. van Veen, D.H.A. Blank, J.F. Vente, J.E. ten Elshof, High-
762 performance hybrid pervaporation membranes with superior hydrothermal and acid stability,
763 *Journal of Membrane Science*. 324 (2008) 111–118.
764 <https://doi.org/10.1016/j.memsci.2008.07.014>.
- 765 [42] H.L. Castricum, G.G. Paradis, M.C. Mittelmeijer-Hazeleger, R. Kreiter, J.F. Vente, J.E. ten Elshof,
766 Tailoring the Separation Behavior of Hybrid Organosilica Membranes by Adjusting the Structure
767 of the Organic Bridging Group, *Advanced Functional Materials*. 21 (2011) 2319–2329.
768 <https://doi.org/10.1002/adfm.201002361>.
- 769 [43] H.M. van Veen, M.D.A. Rietkerk, D.P. Shanahan, M.M.A. van Tuel, R. Kreiter, H.L. Castricum, J.E.
770 ten Elshof, J.F. Vente, Pushing membrane stability boundaries with HybSi® pervaporation
771 membranes, *Journal of Membrane Science*. 380 (2011) 124–131.
772 <https://doi.org/10.1016/j.memsci.2011.06.040>.

- 773 [44] G.G. Paradis, D.P. Shanahan, R. Kreiter, H.M. van Veen, H.L. Castricum, A. Nijmeijer, J.F. Vente,
774 From hydrophilic to hydrophobic HybSi® membranes: A change of affinity and applicability,
775 Journal of Membrane Science. 428 (2013) 157–162.
776 <https://doi.org/10.1016/j.memsci.2012.10.006>.
- 777 [45] M. Khellaf, C. Charcosset, D. Mangin, E. Chabanon, Solubility of L-glutamic acid in concentrated
778 water/ethanol solutions, Journal of Crystal Growth. 570 (2021) 126238.
779 <https://doi.org/10.1016/j.jcrysgr.2021.126238>.
- 780 [46] S.-K. Mah, S.-P. Chai, T.Y. Wu, Dehydration of glycerin solution using pervaporation: HybSi and
781 polydimethylsiloxane membranes, Journal of Membrane Science. 450 (2014) 440–446.
782 <https://doi.org/10.1016/j.memsci.2013.09.048>.
- 783 [47] E. Gagnière, D. Mangin, F. Puel, A. Rivoire, O. Monnier, E. Garcia, J.P. Klein, Formation of co-
784 crystals: Kinetic and thermodynamic aspects, Journal of Crystal Growth. 311 (2009) 2689–2695.
785 <https://doi.org/10.1016/j.jcrysgr.2009.02.040>.
- 786 [48] G. del Campo, J. Zuriarrain, A. Zuriarrain, I. Berregi, Quantitative determination of carboxylic
787 acids, amino acids, carbohydrates, ethanol and hydroxymethylfurfural in honey by ¹H NMR, Food
788 Chemistry. 196 (2016) 1031–1039. <https://doi.org/10.1016/j.foodchem.2015.10.036>.
- 789 [49] H.T. Truong, S. Rode, D. Roizard, S. Mouzon-Pelletier, S. Tretjak, Dehydration of reactive
790 industrial mixtures by pervaporation: An innovative approach in acrylic esters processes,
791 Separation and Purification Technology. 120 (2013) 24–34.
792 <https://doi.org/10.1016/j.seppur.2013.09.017>.
- 793 [50] A.V. Klinov, R.R. Akberov, A.R. Fazlyev, M.I. Farakhov, Experimental investigation and modeling
794 through using the solution-diffusion concept of pervaporation dehydration of ethanol and
795 isopropanol by ceramic membranes HybSi, Journal of Membrane Science. 524 (2017) 321–333.
796 <https://doi.org/10.1016/j.memsci.2016.11.057>.
- 797 [51] S. Sablani, M. Goosen, R. Al-Belushi, M. Wilf, Concentration polarization in ultrafiltration and
798 reverse osmosis: a critical review, Desalination. 141 (2001) 269–289.
799 [https://doi.org/10.1016/S0011-9164\(01\)85005-0](https://doi.org/10.1016/S0011-9164(01)85005-0).
- 800 [52] A. Giacobbo, A. Moura Bernardes, M.J. Filipe Rosa, M.N. De Pinho, Concentration Polarization in
801 Ultrafiltration/Nanofiltration for the Recovery of Polyphenols from Winery Wastewaters,
802 Membranes. 8 (2018) 46. <https://doi.org/10.3390/membranes8030046>.
- 803 [53] F. Zhang, B. Shan, Y. Wang, Z. Zhu, Z.-Q. Yu, C.Y. Ma, Progress and Opportunities for Utilizing
804 Seeding Techniques in Crystallization Processes, Org. Process Res. Dev. 25 (2021) 1496–1511.
805 <https://doi.org/10.1021/acs.oprd.1c00103>.
- 806 [54] Y. He, Z. Gao, T. Zhang, J. Sun, Y. Ma, N. Tian, J. Gong, Seeding Techniques and Optimization of
807 Solution Crystallization Processes, Org. Process Res. Dev. 24 (2020) 1839–1849.
808 <https://doi.org/10.1021/acs.oprd.0c00151>.
- 809 [55] M. Voges, I.V. Prikhodko, S. Prill, M. Hübner, G. Sadowski, C. Held, Influence of pH Value and Ionic
810 Liquids on the Solubility of L-Alanine and L-Glutamic Acid in Aqueous Solutions at 30 °C, J. Chem.
811 Eng. Data. 62 (2017) 52–61. <https://doi.org/10.1021/acs.jced.6b00367>.
- 812 [56] H. Zhang, D. He, S. Niu, H. Qi, Tuning the microstructure of organosilica membranes with
813 improved gas permselectivity via the co-polymerization of 1,2-bis(triethoxysilyl)ethane and 1,2-
814 bis(triethoxysilyl)methane, International Journal of Hydrogen Energy. 46 (2021) 17221–17230.
815 <https://doi.org/10.1016/j.ijhydene.2021.02.139>.
- 816 [57] A.P. Dral, J.E. ten Elshof, Organic groups influencing microporosity in organosilicas, Microporous
817 and Mesoporous Materials. 267 (2018) 267–273.
818 <https://doi.org/10.1016/j.micromeso.2018.03.036>.
- 819 [58] J. Schöll, D. Bonalumi, L. Vicum, M. Mazzotti, M. Müller, In Situ Monitoring and Modeling of the
820 Solvent-Mediated Polymorphic Transformation of L-Glutamic Acid, Crystal Growth & Design. 6
821 (2006) 881–891. <https://doi.org/10.1021/cg0503402>.
- 822 [59] Y. Tahri, E. Gagnière, E. Chabanon, T. Bounahmidi, D. Mangin, Investigation of the L-Glutamic acid
823 polymorphism: Comparison between stirred and stagnant conditions, Journal of Crystal Growth.
824 435 (2016) 98–104. <https://doi.org/10.1016/j.jcrysgr.2015.11.019>.

- 825 [60] Y. Tahri, E. Gagnier, N. Candoni, Multiscale Experimental Study and Modeling of L-Glutamic acid
826 Crystallization: Emphasis on a Kinetic Explanation of the Ostwald Rule of Stages, *Cryst. Growth*
827 *Des.* (2019) 9.
- 828 [61] W. Ostwald, Studien über die Bildung und Umwandlung fester Körper: 1. Abhandlung:
829 Übersättigung und Überkaltung, *Zeitschrift für Physikalische Chemie.* 22U (1897) 289–330.
830 <https://doi.org/10.1515/zpch-1897-2233>.
- 831 [62] Y. Tahri, D. Mangin, Modeling the Competition between Polymorphic Phases: Highlights on the
832 Effect of Ostwald Ripening, *Cryst. Growth Des.* (2016) 9.
- 833